

# THE IONIZED NUCLEAR ENVIRONMENT IN NGC 985 AS SEEN BY CHANDRA AND BEPPoSAX

Y. Krongold<sup>1</sup>, F. Nicastro<sup>1</sup>, M. Elvis<sup>1</sup>, N.S. Brickhouse<sup>1</sup>, S. Mathur<sup>2</sup>, A. Zezas<sup>1</sup>

## ABSTRACT

We investigate the ionized environment of the Seyfert 1 galaxy NGC 985 with a new *Chandra*-HETGS observation and an archival BeppoSAX observation. Both spectra exhibit strong residuals to a single powerlaw model, indicating the presence of an ionized absorber and a soft excess. A detailed model over the *Chandra* data shows that the 0.6-8 keV intrinsic continuum can be well represented by a powerlaw ( $\Gamma \approx 1.6$ ) plus a blackbody component ( $kT=0.1$  keV). Two absorption components are clearly required to fit the absorption features observed in the *Chandra* spectrum. The components have a difference of 29 in ionization parameter and 3 in column density. The presence of the low ionization component is evidenced by an Fe M-shell unresolved transition array (UTA) produced by charge states VII to XIII. The high ionization phase is required by the presence of broad absorption features arising from several blends of Fe L-shell transitions (Fe XVII-XXII). A third highly ionized component might also be present, but the data does not allow to constrain its properties. Though poorly constrained, the outflow velocities of the components ( $581 \pm 206$  km s<sup>-1</sup> for the high ionization phase and  $197 \pm 184$  km s<sup>-1</sup> for the low ionization one) are consistent with each other, and with the outflow velocities of the absorption components observed in the UV. In addition, the low ionization component produces significant amounts of O VI, N V, and C IV which suggests that a single outflow produces the UV and X-ray features. The broad band (0.1-100 keV) continuum in the BeppoSAX data can be parameterized by a powerlaw ( $\Gamma \approx 1.4$ ), a blackbody ( $kT=0.1$  keV), and a high energy cutoff ( $E_c \approx 70$  keV). An X-ray luminosity variation by a factor 2.3 is observed between the BeppoSAX and *Chandra* observations (separated by almost 3 years). Variability in the opacity of the absorbers is detected in response to the continuum variation, but while the colder component is consistent with a simple picture of photoionization equilibrium, the ionization state of the hotter component seems to increase while the continuum flux drops. The most striking result in our analysis is that during both the *Chandra* and the BeppoSAX observations, the two absorbing components appear to have the same pressure. Thus, we suggest that the absorption arises from a multi-phase wind. Such scenario can explain the change in opacity of both absorption components during the observations, but requires that a third hotter component is pressure-confining the two phases. Hence, our analysis points to a 3-phase medium similar to the wind found in NGC 3783, and further suggests that such a wind might be a common characteristic in AGN. The pressure-confining scenario requires fragmentation of the confined phases into a large number of clouds.

## 1. INTRODUCTION

Highly ionized (or ‘warm’) absorbers (Halpern 1982) have been observed in about half of all UV and X-ray spectra of AGNs (Reynolds 1997, George et al. 1998, Crenshaw et al. 1999). The absorption lines of these systems are blueshifted with respect to the optical emission lines, which implies outflow of material. The mass loss rates inferred from these outflows can be a substantial fraction of (Mathur, Elvis & Wilkes 1995) or even larger than (Behar et al. 2003, Ogle et al. 2004) the accretion rates needed to power the AGN continuum, indicating that these ‘quasar winds’ play an important role in the mass and energy budgets of AGNs.

The UV and X-ray absorbers must be closely related, as exactly the same AGNs show both (Mathur, Elvis, & Wilkes 1995; Mathur, Wilkes, & Elvis 1998; Crenshaw et al. 1999; Monier et al. 2001). Furthermore, their kinematic properties also appear to be related, as both absorbers show similar outflow velocities ( $\sim 1000 \text{ km s}^{-1}$ ). Given the intrinsic complexity of UV and X-ray spectra, along with the large difference in spectral resolution in the two bands (with an order of magnitude lower spectral resolution in the X-ray region), it has been extremely difficult to connect these absorbers in detail, leading to highly complicated models to describe them. Nevertheless, recent studies using more comprehensive models have shown that the obser-

vational data are certainly pointing to a common nature for the UV and X-ray outflows (see §5.1).

New studies based on high quality data have shown that the absorbers can be described in a surprisingly simple way. For example, Krongold et al. (2003) modeled the 900 ksec *Chandra* HETG exposure on NGC 3783 (Kaspi et al. 2002) and found that most of the absorption features present in the spectrum could be reproduced by a model with only two absorption components, and that these components appeared to be in pressure balance. This result was confirmed by Netzer et al. (2003), who found a third highly ionized component, also in pressure equilibrium with the other two. Is this single object result only a coincidence? Or, on the contrary, does it suggest that promising advances in our understanding of the physical conditions of AGN winds can be achieved, carrying important repercussions in our understanding of the structure of quasars (e.g. Elvis 2000)?

Here, we present *Chandra* HETG and BeppoSAX observations of the Seyfert 1 galaxy NGC 985 and show that the X-ray spectra of this source can also be well described by a simple model with two absorption components. Furthermore, as for the ionized absorber toward NGC 3783, these components are consistent with pressure equilibrium, with one phase having sufficiently low ionization to produce substantial absorption in the UV region. We further discuss the implications of these results.

---

<sup>1</sup>Harvard-Smithsonian Center for Astrophysics. 60 Garden Street, Cambridge MA 02138

<sup>2</sup>Department of Astronomy, Ohio State University, 140 West 18th Avenue, Columbus, OH 43210

## 1.1. NGC 985

NGC 985 (Mrk 1048) is a Seyfert 1 galaxy located at redshift  $0.04274 \pm 0.00005$  ( $12814 \pm 15$  km s $^{-1}$ ; Arribas et al. 1999, based on stellar absorption features). NGC 985 is a peculiar galaxy with a prominent ring shaped zone at several kiloparsecs from the nucleus (de Vaucouleurs & de Vaucouleurs 1975), suggesting that the galaxy is undergoing a merging process. Further evidence for a merger has been found through optical and near-IR observations, which have revealed the presence of a double nucleus (Perez Garcia & Rodriguez Espinosa 1996, and references therein). The nuclei are separated by 3" (2.5 kpc of projected linear distance; Appleton et al. 2002), which indicates that the intruder galaxy responsible for the formation of the ring is sinking in the nuclear potential of the primary galaxy (Perez-Garcia & Rodriguez-Espinosa 1996). As in other galaxies undergoing a merger, the IR luminosity of NGC 985 is extreme,  $L_{IR} = 1.8 \times 10^{11} L_{\odot}$ , which puts this object in the LIRG group.

An ionized absorber has been observed in the X-ray spectra of NGC 985. This source has been observed in the X-rays with different satellites and is a strong X-ray source. The first detection was with the Einstein Observatory, measuring an 0.2-4.0 keV flux of  $1.76 \times 10^{-11}$  erg s $^{-1}$  cm $^{-2}$  (a luminosity of  $1.4 \times 10^{44}$  erg s $^{-1}$ ; Kruper, Urry, & Canizares 1990). Subsequently, spectral analysis of ROSAT-PSPC data revealed complex features (Brandt et al. 1994). A simple power law could not fit the PSPC spectrum of NGC 985, and the presence of a warm absorber, as well as a continuum soft excess, was suggested. In

1996, NGC 985 was observed by ASCA with a total exposure of 40 ksec. The analysis of these data confirmed the presence of an ionized absorber in the spectra of this source (Nicastro et al. 1998, 1999). Nicastro et al. found that photoelectric bound-free edge absorption could not account for all the features observed, and suggested that resonant bound-bound line absorption played an important role.

This possibility was supported by HST-STIS and FUSE ultraviolet observations of the nucleus in NGC 985, which have revealed the presence of six narrow absorption components detected in Ly  $\alpha$ , C IV, N V and O VI (Arav 2002). Five of these systems are observed in outflow, with velocities (with respect to the centroid of the narrow emission lines) of 780, 670, 519, 404, and 243, km s $^{-1}$  (hereafter components 1 to 5). The sixth component is observed inflowing at  $-140$  km s $^{-1}$ . As demonstrated by Arav, small to moderate saturation is present in the Ly  $\alpha$  trough of these components. Once the effects of saturation are accounted for, at least component 4 is consistent with gas that also produces X-ray absorption, i.e. a highly ionized or 'warm' absorber, with a column density of  $10^{21.4}$  cm $^{-2}$ .

In this paper we present 2 moderate exposure observations of NGC 985 ( $\sim 100$  ksec each) with *Chandra* and BeppoSAX. In §2 we describe the reduction and spectral analysis of the *Chandra*-HETGS data. The analysis was carried out in Sherpa<sup>1</sup> (Freeman, Doe, & Siemiginowska 2001), with the inclusion of the code PHASE (Krongold et al. 2003) to model in a self-consistent way the ionized absorber present in the spectra. In §3 we present the

BeppoSAX data, and in §4 we analyze the variability effects of the source on the absorber. In §§5 and 6 we discuss the different scenarios consistent with the absorber and their implications.

## 2. THE *Chandra*-HETG SPECTRUM

On 2002 June 24, the High Energy Transmission Grating Spectrometer (HETGS, Canizares et al. 2000) on board the *Chandra* X-ray Observatory (Weisskopf et al. 2000) observed NGC 985 (see Table 1). The observation was carried out with the Advanced CCD Imaging Spectrometer (ACIS; Garmire et al. 2003) in the focal plane, and had a duration of 80 ksec. We processed the event files of this observation with the *Chandra* Interactive Analysis of Observations (CIAO<sup>2</sup>; Fruscione 2002) software (Version 2.3), following the on-line data analysis “threads” provided by the *Chandra* X-ray Center (CXC<sup>3</sup>), and extracted source and background 1st order spectra (positive and negative orders) and responses for the High-Energy Grating (HEG) and Medium-Energy Grating (MEG) configurations. We accounted for the ACIS efficiency degradation (Marshall et al. 2003) using the script *contamabs*<sup>4</sup> (version 1.1). The net exposure of the observation is 77.7 ksec and the total number of counts in the dispersed spectrum is 13,979.

We then combined the -1st and +1st or-

der spectra to improve the signal to noise (S/N) ratio of the data. Similarly, after checking for wavelength scale consistency, the HEG and MEG spectra and their responses were coadded in the overlapping region, to further increase the S/N ratio. The S/N ratio per MEG resolution element ( $\approx 0.02$  Å) varies from  $\approx 7$  to  $\approx 2$  in the 2-20 Å range, a factor  $\approx 6$  lower than the highest S/N ratio HETG spectrum of a Sy 1 galaxy (NGC 3783; Kaspi et al. 2002). All the spectra presented throughout the paper (except where otherwise stated) correspond to a binning factor of 20 (i.e we binned the spectrum in bins of size 0.1 Å, about 5 times the MEG resolution element), giving a S/N ratio ranging from 14 to 3 per bin (in the 2-20 Å range). The spectrum is shown in Figure 1a.

### 2.1. Spectral Analysis

In the calculations reported here, we attenuated the continuum by an equivalent hydrogen column density of  $3.0 \times 10^{20}$  cm<sup>-2</sup> to account for the Galactic absorption by cold gas in the direction to the source (Starck et al. 1992). We have explored only photoionization equilibrium models, and we have assumed solar elemental abundances (Grevesse & Noels 1993).

#### 2.1.1. Fitting the Continuum

To model the intrinsic continuum of the source, we first used a simple power law. This model could not fit the data over the entire energy range (0.6-8 keV, 1.5-20 Å), as can be seen from the residuals (Fig. 2a). The model shows both positive and negative deviations (with significance  $> 2\sigma$ ) typical of the ionized absorber and soft excess commonly observed in Seyfert 1 galax-

<sup>1</sup><http://cxc.harvard.edu/sherpa>

<sup>2</sup><http://asc.harvard.edu/ciao>

<sup>3</sup><http://asc.harvard.edu/ciao/documents.threads.html>

<sup>4</sup>[http://space.mit.edu/CXC/analysis/ACIS\\_Contam/ACIS\\_Contam.html](http://space.mit.edu/CXC/analysis/ACIS_Contam/ACIS_Contam.html)

ies (e.g. Reynolds 1997).

We repeated the power law fit using only data between 3 and 8 keV (we also excluded the Fe K $\alpha$  line region around 6.4 keV). At these energies, absorption by moderately large columns of ionized gas (i.e.  $< 10^{23} \text{ cm}^{-2}$ ) or low columns of neutral gas (i.e.  $< 10^{21} \text{ cm}^{-2}$ , Galactic gas) do not modify significantly the shape of the intrinsic continuum (e.g. Krongold et al. 2003). The results of this model are summarized in Table 2, and the residuals (extrapolated to the whole spectral range) are presented in Figure 2b. The presence of strong positive and negative deviations below 3 keV in this model shows that both an ionized absorber and a soft excess are likely to be present. To account for the presence of the excess, we further included a blackbody component in our continuum determinations, and the positive residuals decreased significantly (see Fig. 2c). However, the model still shows strong negative residuals at energies characteristic of an ionized absorber.

Finally, we fitted the continuum and the absorption together (see §2.1.2 for the details of the ionized absorber). In this model we left all the continuum components (power law and blackbody) free to vary, and we assumed that the absorbing gas also covers the soft excess. The results obtained for the power law with this approach are in excellent agreement with the results obtained when considering only the 3-8 keV range. Table 2 presents the values for the best continuum fit. Figure 1a shows the fluxed data over the entire spectral range (1.5-20 Å, 0.6-8 keV), together with (a) the intrinsic continuum of the source, (b) the continuum attenuated

by Galactic absorption, and (c) the observed continuum (i.e. the continuum further attenuated by the bound-free transitions from the ionized absorber, see details in Fig. caption).

### 2.1.2. Modeling the Ionized Absorber

We ran PHASE with three free parameters for each component necessary to fit the ionized absorber: (1) the ionization parameter (defined over the entire Lyman continuum, as  $U = Q(H)/4\pi r^2 n_H c$  with  $Q(H)$  being the rate of H ionizing photons,  $r$  the distance to the source,  $n_H$  the H density, and  $c$  the speed of light.), (2) the equivalent hydrogen column density  $N_H$ , and (3) the outflow velocity. Other parameters of the code that we kept fixed are the internal micro-turbulent velocity of the absorbers and the intrinsic Spectral Energy Distribution (SED) of the source (Fig. 3a). The turbulent velocity of the gas is very difficult to constrain, since (1) single absorption lines in the spectrum are unresolved by the HETGS (which has a FWHM resolution of  $\approx 400 \text{ km s}^{-1}$  at 17 Å) and (2) most of the observed features are blends of several transitions. We set this parameter to  $350 \text{ km s}^{-1}$ , the value most suitable to the data after several tests comparing the measured equivalent widths (EWs) of a few unblended lines (Si XIV, Si XIII, Mg XII, Mg XI, Fe XVII) with the EWs predicted by our model.

To approximate the SED, we proceeded as follows: in the X-ray region we used the power law  $\Gamma$ , as well as the blackbody contribution, as inferred from the fits to the continuum presented in §2.1.1. To obtain the exact parameters for the blackbody component several iterations were

performed. The BeppoSAX data of NGC 985 show the presence of a high energy cut-off in the intrinsic continuum (see §3.1.1), which we modeled with a break in the X-rays at around 70 keV, and a powerlaw with  $\Gamma = 5$  above this energy. Based on HST-STIS observations of NGC 985, Bowen, Pettini & Blades (2002) found a flux of  $2.54 \times 10^{-26}$  erg s $^{-1}$  cm $^{-2}$  hz $^{-1}$  at 1230 Å. In order to determine the flux at the Lyman limit, we extrapolated to 912 Å assuming a power law with photon index  $\Gamma = 2$ . The flux at 912 Å turned out to be  $1.83 \times 10^{-26}$  erg s $^{-1}$  cm $^{-2}$  hz $^{-1}$ . Extrapolation of the X-ray continuum down to the Lyman limit gives a flux two orders of magnitude smaller than measured by HST, which indicates the presence of a soft X-ray-UV energy break, with a steepening of the spectrum between the two bands (Fig. 3a). We assumed that this break occurs at 0.1 keV. The actual energy of this break is unknown (due to the unobservable region in the UV-X-ray range associated with Galactic absorption). We restricted the SED at low energies using (not simultaneous) data from NED<sup>5</sup> (see Fig.3a). For simplicity we extended the extrapolation between 1230 Å and 912 Å up to 100  $\mu$ m (i.e. we considered a power law with  $\Gamma = 2$  from 912 Å to 100  $\mu$ m). Below 100  $\mu$ m we introduced a low energy cut-off with  $\Gamma = -3.5$ . The final SED used to model the *Chandra* data is presented in Figure 3a. The differences in the infrared region between NED data and our assumed SED do not have any effect on our analysis (the only effect such differences produce is an increase of the Compton temperature by a factor  $< 1.1$ , when the NED data are

considered).

### 2.1.3. The Ionized Absorber

As is the case for other ionized absorbers in AGNs (Kaspi et al. 2001; Blustin et. al 2002; Krongold et al. 2003; Netzer et al. 2003 for NGC 3783; Kaastra et al. 2002 for NGC 5548; Steenbrugge et al. 2003 for NGC 4593; Blustin et al. 2003 for NGC 7469) the ionized absorber in the spectrum of NGC 985 could not be well fitted by a single absorbing component ( $\chi^2/\text{d.o.f.} = 201.6/177$ ). Therefore, we attempted to fit the spectrum with the next simplest model, by including a second component. In this case, we obtained an acceptable fit to the data ( $\chi^2/\text{d.o.f.} = 179.03/174$ ; an F-test indicates that the second component is required at a significance level larger than 99.9%). Table 3 lists our results, and the best fitting model is presented in Figure 4 (and also in Fig. 1b, where we show the model for the full spectral range plotted over the fluxed spectrum). Most of the narrow features observed in Figure 4 have a significance  $< 2\sigma$ , but still the absorber is clearly detected and constrained through the presence of relatively broad features due to both photoelectric bound-free absorption and blends of resonant bound-bound transitions (i.e. Fe L-shell and Fe M-shell absorption). To highlight the presence of these features (which are significant at a level  $> 2.5\sigma$ ), in Figure 5 we present our model and the data in the 12-18 Å range, with a binning size of 0.15 Å (binning factor of 30).

Two different ionization absorbing com-

---

<sup>5</sup>NASA/IPAC Extragalactic Database,  
<http://nedwww.ipac.caltech.edu>

ponents are clearly required by the data. The presence of significant features produced by both Fe L-shell transitions (Fe XVII-XXII) and Fe inner M-shell transitions (Fe VII-XIII, the unresolved transition array or UTA) is incompatible with a single ionization degree for the absorbing gas. This is shown in Figure 6, where the contribution from the two components to the absorption is presented separately. The high ionization phase (hereafter HIP), with  $\log U = 1.34$ , gives rise to the absorption by O VIII, Ne IX-X, Mg XI-XII, Si XIII-XIV, and Fe L-shell. The low ionization phase (hereafter LIP), with  $\log U = -0.12$ , is responsible for the absorption by charge states O VII, Ne V-IX, Mg IX, and the Fe M-shell UTA. The components are well separated in ionization degree, the HIP has a value  $\approx 29$  times larger in U than the LIP. Accordingly, the HIP has a higher temperature ( $\log T = 5.8$  [K]) than the LIP ( $\log T = 4.5$  [K]) by a factor of 21. These temperatures were calculated assuming photoionization equilibrium in each component. Figure 7 shows the theoretical spectral features predicted for the absorption components. Table 5 presents the predicted column densities for the dominant charge states in the LIP and the HIP.

As has been observed in other ionized absorbers (see above), the HIP has a larger equivalent H column density than the LIP, in the case of NGC 985 by a factor of 3. The outflow velocity of the components is  $581 \pm 206$  km s $^{-1}$  for the HIP and  $197 \pm 184$  km s $^{-1}$  for the LIP. These velocities, though ill-determined, are consistent with each other (within  $\sim 1\sigma$ ) and with those observed in the HST and FUSE systems (see Fig. 8 for more details). A fit

fixing the velocity of both HIP and LIP at the velocity of the strongest UV component (4, outflowing at 404 km s $^{-1}$ ; see §1 and Fig. 8) yields an acceptable fit to the data, with parameters fully consistent with those obtained before.

In the former analysis we have assumed that the soft excess detected in the data is covered by the absorber. Soft X-ray excesses have been studied in low resolution spectra for more than a decade (e.g., Elvis et al. 1991, and references therein) and they have been found to vary on timescales of tens of days. This effect has been confirmed in high resolution spectra (Netzer et al. 2003), and suggests that the bulk of the soft X-ray emission comes from a compact region (less than  $10^{16}$  cm across; Elvis et al. 1991). It has been suggested that the emission might have a thermal nature and might originate in the inner edges of accretion disks (e.g. Czerny & Elvis 1987). Therefore, it is reasonable to assume that the absorbing material lies further away from the central engine than the soft X-ray emission. Nevertheless, we note that the data does not allow to distinguish whether the soft component is covered by the absorber or not. A fit assuming an uncovered excess is statistically indistinguishable from a fit which assumes full covering. If the excess is not absorbed, then the column density of the LIP is 1.6 times larger and the normalization of the blackbody 2.3 times smaller. The rest of the parameters in this model are fully consistent with the values obtained before. We stress that whether the soft excess is covered or not covered by the absorber, this has a negligible effect on the conclusions presented in this paper.

We find no significant evidence of an ionized emitter in the spectrum. Resonant and forbidden OvII lines have a statistical significance  $\lesssim 1$  sigma. We estimate upper limits for the equivalent width of 218 mÅ for the resonant line and 185 mÅ for the forbidden line. Although an emitter might be present, better data are required for its detection.

## 2.2. Constraining the Ionized Absorber

Despite the limited S/N ratio of the *Chandra* spectra, the physical properties of the ionized absorber in NGC 985 can be constrained. As demonstrated by Behar, Sako, & Kahn (2001) and Krongold et al. (2003), the UTA is a robust indicator of the ionization level of the gas, as the general shape and position of this feature strongly depend on U for a given ionization component. The 12-15 Å Fe L-shell absorption complex also helps to limit the physical state of the gas.

To illustrate this point, we have constructed a series of models with ionization parameters different from those deduced for our best fitting model (see §2.1.3 and Table 3). The comparison of these models with the data reveals clear discrepancies (see Fig. 9). The first model we considered is presented in Figure 9a, and consists of a factor 3 less ionized HIP ( $\log U=0.8$ ). In this model, lower charge states of Fe would be significantly present in the HIP (e.g. Fe xv-xvi), and these would produce abundant Fe M-shell UTA absorption at wavelengths between 15 and 16 Å (see Fig. 9a). This is clearly not observed in the data. At the same time, the deep absorption feature observed in the data around 12.85 Å

(arising from Fe xix-xx), is missing in the model. Thus, the HIP cannot contain less ionized gas.

The ionization state of the LIP is also limited by the data, particularly by the UTA. Figure 9b shows the comparison of the data with a second model that includes a factor 4 more ionized LIP ( $\log U=0.5$ ). This model shows an excess of absorption at 15- 16 Å produced by Fe xiv-xv, and a lack of absorption at longer wavelengths (due to a diminished fraction of Fe in charge states vii-x). A third model consisting of a factor 5 less ionized LIP ( $\log U=-0.8$ ) is presented in Figure 9c. This model is inconsistent with the data also. A low value of U shifts the UTA to higher wavelengths (peak of absorption at 17 Å) because an important fraction of Fe is now present in charge states iv-vi. At the same time, the lack of Fe x-xii produces an underestimation of the absorption around 15.9-16.4 Å. From this analysis is evident that even lower values of U for the LIP ( $\log U < -0.8$ ) would produce even more shifted UTAs (produced by even lower Fe charge states), and therefore, higher discrepancies between data and model. Thus, the data impose important restrictions on the ionization state of the absorbing gas.

A third absorber with an intermediate value of the ionization parameter (between the HIP and the LIP) and high H column density can also be ruled out. Figure 9d illustrates the inconsistencies that arise when a third absorber with  $\log U=0.6$  and  $\log N_H=21.5$  [cm<sup>-2</sup>] is included in our model. Such an absorber severely overpredicts the absorption by the UTA from 15 to 16 Å (because of a high contribution to the absorption in the model by Fe xiv-

xvi). However, it is not possible to rule out the presence of additional absorbing components with lower H column density.

To quantify the limits imposed by the data to additional absorbing material we included a third absorption component in our model and refit the data. In Figure 10a we show the  $\log U$ - $\log N_H$  confidence region for this hypothesized absorber. The plot shows that gas with  $U$  between the HIP and the LIP and  $\log N_H > 21.1$  [ $\text{cm}^{-2}$ ] (half the column density of the LIP and 20% that of the HIP) can be ruled out (at the  $3\sigma$  level). Figure 10a also shows that the presence of material less ionized than the LIP and  $\log N_H > 21$  [ $\text{cm}^{-2}$ ] can also be ruled out (at  $3\sigma$  significance).

On the other hand, a third component with very high ionization parameter and considerable column density can be present in the spectra of NGC 985. Figure 10b presents the confidence region for a 3rd component consisting of high column density and high ionization gas. As observed in the figure such a component is not well constrained by the data, but in order to have larger column density than the HIP ( $\log N_H > 21.8$  [ $\text{cm}^{-2}$ ]) requires  $\log U > 2$  (i.e. 5 times larger  $U$  than the HIP). In fact the discrepancies (with significance  $< 2\sigma$ ) between 1.6 and 1.7  $\text{\AA}$ , and near 10.6  $\text{\AA}$  (see Fig. 11) hint at the presence of such material, as they are consistent with absorption by Fe XXIV-XXVI.

It is clear, then, that the gas tends to clump in two different degrees of ionization, with the majority of the low ionized material around the LIP. A third, very high ionization component is hinted at by the data, but better S/N ratio data are needed to establish its existence and constrain its

physical properties.

### 2.2.1. The Effects Induced by the Lack of Accurate Dielectronic Recombination Rates

Our analysis of the LIP is based mostly on the Fe M-shell UTA, and low temperature Dielectronic Recombination Rate (DRR) coefficients have not been calculated or measured yet for these ions. Krongold et al. (2003) and Netzer et al. (2003) reported that the models were unable to simultaneously reproduce the absorption by the UTA and two lines of Si (Six at  $\lambda 6.850$  and SixI at  $\lambda 6.775$ ). Netzer et al. (2003) proposed that this was an effect introduced by the lack of these DRR. This means that, for a given value of the ionization parameter, there is a systematic shift in the ionization balance of Fe (toward higher charge states) with respect to the rest of the species. Netzer (2004) and Kraemer, Ferland, & Gabel (2004) have estimated these rates. Their results show that there is indeed an increase in the ionization parameter at which the Fe M-shell ions peak, offering a solution for the mismatch between the UTA and Si lines in the spectrum of NGC 3783.

In the spectrum of NGC 985, besides the UTA, there are no other significant absorption features that allow us to constrain the ionization parameter of the LIP. Accepted at face value, this means that we are underestimating the ionization parameter (and temperature) of the LIP, because of the lack of Fe M-shell DRR. However, from our previous analysis on NGC 3783 (Krongold et al. 2003), we estimate that the error cannot exceed a factor of 2 in  $U$  (i.e.  $\Delta \log U < 0.3$ ), a factor consistent with

the one obtained by Netzer et al. (2003) and Kramer, Ferland, & Gabel (2004). We have repeated our analysis shifting up by a factor of 2 the ionization parameter of the LIP in all elements except Fe. With the quality of the present data, this distinction does not modify our results in any significant way. In fact, estimates with this new approach of the column density and ionization parameter of possible additional absorbing components yield to limits fully consistent with those presented in the former section, showing again that the gas clumps in two, or maybe three, absorbing components.

While our main conclusions will not change due to this underestimation of  $U$ , this effect should be kept in mind. Therefore, we have set the positive error bar in the ionization parameter of the LIP to be consistent with a factor of 2 change in  $U$ , in order to reflect the underestimation introduced by the lack of low temperature DRR for Fe.

Recent calculations by Gu et al. (2003), and measurements by Savin et al. (2002a, 2002b, 2003) have produced more accurate values for Fe L-shell DRR. At temperatures close to the one derived for the HIP  $\sim 10^6$  K ( $\sim 86$  eV) the differences between the old estimates and the new ones are relatively small (although these differences become larger at lower temperatures, i.e.  $10^5$  K). Thus, although the new calculations have not been incorporated into the photoionization codes, we expect the uncertainties introduced into the HIP model by the uncertainties of the Fe L-shell DRR currently used in the codes to be within the error bars derived in our analysis. In fact, our model for this component is able

to fit the Fe L-shell lines, along with K-shell lines arising from other elements, like Si, Mg, and Ne (see Fig. 4). Although the significance of these narrow lines is limited, it is clear that the ionization state of the gas is consistent with the observed charge states. We note that the same was found for the high S/N ratio spectrum of NGC 3783 (Krongold et al. 2003; Netzer et al. 2003). Therefore, we do not expect a systematic underestimation of  $U$  in the HIP.

### 3. BeppoSAX DATA

To further study the nature of the ionized absorber, in particular to constrain the absorber response to the changes in the continuum of the central source, we retrieved and reprocessed the previously unpublished NGC 985 data obtained by BeppoSAX (Boella et al. 1997; Piro et al. 1997) on 1999 August 29 (see Table 1). The data have a total MECS exposure of 90 ks. We followed the standard reduction procedure (Fiore et al. 1999) for the LECS, MECS, and PDS data. We extracted LECS and MECS source spectra from circles of radius 8' and 4' respectively, and the same extraction regions were used to extract background spectra from the LECS and MECS "blank fields." The PDS instrument has no imaging capability and is a collimated detector with a field of view (FOV) of  $1^{\circ}.3$  (FWHM). It makes use of rocking collimators for background monitoring. Using the ROSAT All Sky Survey, we searched the FOV of the PDS in the direction to NGC 985, and did not find any other source in this region capable of a significant contamination of the PDS spectrum (Mrk 1044 is the closest bright X-ray source to NGC 985 in the sky, at an angu-

lar distance of  $1.2^\circ$ , but it was outside the FOV of the PDS during the observation).

Modest variability was observed during the BeppoSAX observation of NGC 985. In the 0.1-2.0 keV band (LECS data), source variations were detected up to a factor 1.45 on a time-scale of about 50 ksec. Variability in the 2.0-10 keV range (MECS data) was detected up to a factor of 1.3 in the same time-scale. The quality of the data does not allow for a separation in low and high state spectra, therefore we modeled the full time integrated dataset.

### 3.1. Spectral Analysis

#### 3.1.1. Fitting the Continuum

To model the broadband (0.1-100 keV) BeppoSAX continuum of NGC 985, we first followed the same approach used with the *Chandra* data, constraining the intrinsic powerlaw in the 3-8 keV range. The residuals of the extrapolation of this model to the whole BeppoSAX band are presented in Figure 12. The presence of both an ionized absorber and a soft excess is evident, together with that of a high energy cutoff at energies larger than 60 keV. We then refitted the data including an exponential cutoff to model the continuum at high energies, as well as a blackbody and an ionized absorber (see §3.1.2) to model the soft excess and the absorption at low energies.<sup>6</sup> Results of our best continuum fits are shown in Table 2. The intrinsic continuum of the source further attenuated by Galactic absorption is shown in Figure 13a (dashed line).

---

<sup>6</sup>The inclusion of a cold reflector, often observed in the high energy spectra of Seyfert galaxies (e.g. NGC 3783, Kaspi et al. 2001, de Rosa et al. 2002),

The BeppoSAX data indicate a flatter power law photon index ( $\Delta\Gamma \approx 0.2 \pm 0.07$ ) and a larger flux in both the power law and the blackbody components (by a factor  $\approx 2.3$ ) with respect to the *Chandra* data. These differences are reflected in the SED used to fit the ionized absorber in the BeppoSAX data (see Fig. 14).

#### 3.1.2. Modeling the Ionized Absorber Present in the BeppoSAX Data

Modeling of absorption features in low resolution data is extremely difficult because the lack of detail does not allow the determination of the exact ionization state of the gas and the number of absorbing components. Because of this, we decided to use the solution found for the high resolution *Chandra* data, to constrain the physical properties of the gas at low resolution. We assumed that two components contribute to the absorption, as inferred from the *Chandra* data, and fixed the outflow velocity and the turbulent velocity of the absorbers to the values deduced in §2.1.3 (these parameters are essentially unconstrained when modeling low resolution data).

First, we left the ionization parameter and the column density of both components free to vary while fitting the data. An acceptable fit was obtained (reduced  $\chi^2 = 1.063$  for 112 degrees of freedom), with column density values in both absorption components closely consistent with the values obtained modeling the *Chandra* data: we find column density values of

---

is not required by the BeppoSAX data of NGC 985. We find a  $2\sigma$  upper limit for the amount of reflection  $R < 0.7$ , see Table 2.

$\log N_H = 21.95 \pm 0.24$  [cm $^{-2}$ ] ( $\Delta \log N_H = 0.14$  [cm $^{-2}$ ]) for the HIP and  $\log N_H = 21.38 \pm 0.26$  [cm $^{-2}$ ] ( $\Delta \log N_H = 0.01$  [cm $^{-2}$ ]) for the LIP. Hence, we next froze the column densities to the values obtained with *Chandra*, and fit the data letting only the ionization parameters vary. The results are reported in Table 4, and are discussed in the next section. Figure 13 shows the data and the best fit model and Table 5 shows the predicted column densities for the dominant charge states.

## 4. VARIABILITY ANALYSIS

### 4.1. Intensity and Spectral Changes in the Continuum

A comparison of the 2002 *Chandra* and 1999 BeppoSAX observations indicates a flux drop by a factor of 2.3 in the 0.1-10.0 keV range. Variability is observed in both the soft X-ray (0.1-2.0 keV) and hard X-ray (2.0-10.0 keV) bands. Since the hard X-ray region is barely affected by the ionized absorber, the change of flux is indicative of intrinsic source variations. Our continua fits indicate a steepening in slope of  $\Delta\Gamma \approx 0.2 \pm 0.07$ . Any attempt to fit both datasets with a single photon index value yields unsatisfactory results. For instance, we find a  $\chi^2 = 59.1$  for 50 degrees of freedom when fitting (between 3 and 8 keV) the *Chandra* data with a value of  $\Gamma$  frozen to 1.4, this imply a  $\Delta\chi^2 = 12.4$  with respect to the best fitting model (an F-test gives a significance larger than 99.9% for this difference). Fitting the BeppoSAX data with a photon index equal to 1.6 produces even worse results. This difference could be indicating a real slope variation or could be the result of cross-calibration

effects between the two instruments. We will follow the analysis assuming  $\Gamma = 1.4$  for the BeppoSAX data, noticing that this difference does not have a significant effect on our conclusions.

To investigate the significance of the variability of the soft emission component, we attempted to fit the BeppoSAX data while freezing the blackbody component used to parameterize the soft excess to the values obtained for our best fitting *Chandra* model. Every model tried imposing this constraint led to an underestimate of the continuum level below 1 keV, pointing to a genuine variation of the flux of the soft component between the two observations. We note from Table 2 that only a change in the intensity of the emission is required by the data, as the best fit solutions to both datasets are consistent with a blackbody temperature of 0.1 keV.

### 4.2. Changes in the Opacity of the Ionized Absorber

The ionization degree of the ionized absorber along the line of sight to NGC 985 has also changed between the *Chandra* and BeppoSAX observations. An F-test comparing the opacities deduced from the *Chandra* best fitting model with those for the BeppoSAX best fitting model shows that the difference is statistically significant at the 99% confidence level. To better quantify the changes in the ionized material, it is convenient to introduce a different ionization parameter,  $U_x$ , defined through the number of ionizing photons between 0.1 and 10.0 keV (Netzer 1996). This definition makes the changes in the ionization parameter (now relevant only to the X-ray species) directly proportional to the

change in the X-ray flux, as opposed to bolometric flux changes, which are not directly observable. Thus, it is preferable in studies of the effects of flux variability over ionized gas in the X-ray regime. The two different definitions of the ionization parameter scale as  $\log U_x = \log U - 2.43$  for the *Chandra* SED, and  $\log U_x = \log U - 2.08$  for the BeppoSAX SED.

The best fit to the *Chandra* data gives a value of  $\log U_x = -2.55 \pm 0.09$  for the LIP. If the gas is in photoionization equilibrium and is not physically confined, a change of flux by a factor 2.3 would induce a change in the X-ray ionization parameter by the same factor, yielding a value of  $\log U_x = -2.20$ . The best fit value of  $\log U_x$  for the BeppoSAX data is  $-2.30 \pm 0.10$ , consistent with the predicted value. We conclude that the LIP is responding to the changes in the continuum and thus is probably both photoionized and in equilibrium.

The value of  $\log U_x$  for the HIP in the *Chandra* data model is  $-1.09 \pm 0.10$ . If the absorber is in equilibrium, the flux change observed between observations implies a value of  $\log U_x = -.73$  for the HIP present in the BeppoSAX spectrum. The value obtained in our best model for the BeppoSAX data is  $\log U_x = -1.25 \pm 0.13$ . These two values of the ionization parameter are clearly inconsistent with each other. Thus, this component has indeed changed ionization state between the two observations, but does not seem to be following the changes on the continuum. On the contrary, the degree of ionization of this gas seems to have increased while the flux decreased.

Such behavior has several possible explanations. (1) The gas is out of equilibrium: the photoionization equilibrium

time scale is inversely proportional to the density in the gas during both increasing and decreasing flux intensity phases (e.g. Nicastro et al. 1999). If the density is low enough, this timescale can be larger than the variability timescale of the central source, and the medium does not have time to adapt to the changes in the continuum. In such conditions, delays in gas responses may lead to scenarios where the ionization degree of the gas decreases while the flux increases. Such cases have been already found in other ionized absorbers around AGN, for instance NGC 4051 (Nicastro et al. 1999). (2) The gas is not in photoionization equilibrium because another mechanism, collisional ionization (due, for instance, to shock heated gas) dominates. In this case, obviously, changes in the gas opacity are essentially unrelated to changes in the source flux. (3) The gas is indeed in photoionization equilibrium, and has undergone a significant change in its density. This is possible if the gas is pressure confined by an external medium. (4) Finally, it is possible that the absorbing gas is not the same during the two observations. X-ray absorbers can change independently of flux variations (see George et al. 1998) because of transverse motion of the material or because of condensation and dissipation of clouds out of a hot medium (Krolik & Kriss 2001). In the following sections we will explore further the validity of these different scenarios.

## 5. ABSORBER PHYSICS DISCUSSION

The ionized absorber present in NGC 985 is suggestive of a simple picture, being constrained by two strong absorption com-

ponents. The same situation was found for the ionized absorbers in IRAS 13349+2438 (Sako et al. 2001) and NGC 3783 (Krongold et al. 2003). In all three objects, an Fe VII-XIII UTA and several OVII lines are the signature of the cooler phase, and the OVIII and Fe XVII-XXII are the main features of the hotter phase, with high ionization iron dominating the spectrum below 15 Å. These ionized absorbers are inconsistent with substantial amounts of material with intermediate values of the ionization parameter. Furthermore, the ionization degree of the LIP is consistent with a cooler medium producing significant amounts of O VI and other lower ionization species, which should also imprint their signature in the UV band (see also §5.1). In the case of NGC 3783, a third very high ionized component has also been detected (Netzer et al. 2003). In NGC 985 the presence of such component is hinted by the data, although it cannot be well constrained (see Fig. 11).

The similar characteristics in the absorbers of these objects suggest that this an intrinsic property related to the structure of the nuclear environment. In the following sections, a possible scenario regarding the nature of these absorbers is discussed.

### 5.1. The UV X-ray Connection of the Absorbers

NGC 985 has been observed with HST-STIS and FUSE. Arav (2002) modeled these data, and showed that, once saturation is accounted for, the component outflowing at 404 km s<sup>-1</sup> (i.e. component 4) produces absorption in the X-ray band.

In Table 6 we present the O VI, N V,

C IV, and H I column densities inferred from the LIP of our *Chandra* best fitting model. It is evident that this absorbing component would produce absorption in the UV band. Arav (2002) measured column densities of  $\log N_{Nv} = 14.2$  [cm<sup>-2</sup>], and an  $\log N_{H_I} = 14.7$  [cm<sup>-2</sup>]. These values are smaller than the ones derived from our model by factors 29 for N V and 5 for H I (see Table 6). Finding consistent column densities for the UV and X-ray absorbers has been historically difficult as has been discussed by Krongold et al. (2003). In the case of NGC 985, a few reasons can be responsible for the discrepancy: (1) The predicted column densities inferred by any model in the UV strongly depend on the exact shape of the SED assumed in the analysis (Kaspi et al. 2001; Steenbrugge et al. 2003). Thus, the overestimation in the model could be an effect induced by our chosen SED (Fig. 3a). In fact, the derived factors reduce to 15 for N V and 4 for H I when considering the SED presented in Figure 3b (see Table 6). The reason for the decrease in ionic column density in this SED is that it has a larger number of photons in the extreme UV, the relevant region for the abundances of the ions absorbing in the UV (note the small decrease in H I, since the photon flux assumed in both SEDs at 912 Å is the same). However, the intrinsic SED in this region cannot be constrained due to Galactic absorption. (2) In addition to SED effects, the fact that the observations are not simultaneous should be kept in mind. It is possible that the absorber has changed in opacity because the gas responds to flux variations (or because the absorbing gas is not the same at the two different epochs). For instance, the ionization parameter for the LIP in the

BeppoSAX model is larger than the one in the *Chandra* model. Then, the difference in N v column density between Arav's measurements and our BeppoSAX best fit model is only 13, if the SED presented in Fig. 14 is used (this SED is similar in the extreme UV to the one presented in Figure 3a for the *Chandra* analysis, with a small flux in this region). Therefore, the different columns can reflect only the ionization state of the gas. (3) Finally, it is possible that other UV components (besides component 4) contribute to the absorption observed in the X-rays.

Quantifying these differences would require simultaneous UV and X-ray observations with high resolution and high S/N ratio. However, we note that NGC 985, along with NGC 5548 (Kaastra et al. 2002; Arav et al. 2003; Steenbrugge et al. 2003), NGC 3783 (Kaspi et al. 2001; Gabel et al. 2003; Krongold et al. 2003; Netzer et al. 2003), and NGC 7469 (Blustin et al. 2003; Kriss et al. 2003) are good examples of the UV and X-ray absorbing connection.

## 5.2. Density and Location of the Absorbing Gas

Our analysis of the LIP indicates that this gas may be in photoionization equilibrium and responding consistently to the changes in the continuum. Using the elapsed time between the high state and low state observations (1029 days) as an upper limit to the recombination time, a lower limit on the density of the recombining gas and an upper limit on the distance from the central source can be set for this gas. For this calculation, we used the photoionization equilibrium temperature, the flux in the 0.1-10 keV range

derived from our fit to the *Chandra* observation, the ionization parameter  $U_x$ , and the recombination rate for OvII (Shull & van Steenberg 1982) since it is the dominant charge state. We estimate a lower limit for the electron density of the LIP of  $n_e(\text{LIP}) > 610 \text{ cm}^{-3}$ . This translates into an upper limit of  $R(\text{LIP}) < 21.6 \text{ pc}$  for the distance between the central source and the ionized gas, and a maximum thickness  $\Delta R(\text{LIP}) < 1.3 \text{ pc}$  for the gas.

## 5.3. Thermal Instabilities and the Absorbing Components

Several models have been proposed to explain the nature of the ionized absorbers around AGN. The different scenarios include a continuous range of ionization parameters (Krolik & Kriss 2001), different clouds in different regions (including for instance different UV and X-ray absorbing regions), or similar locations for the absorbing winds (Krongold et al. 2003).

The data presented here suggest that a continuous range of  $U$  does not adequately describe the observed spectra (see discussion in §2.2). The presence of different clouds in different regions seems unlikely (at least for the objects discussed here), not only because of the similar characteristics of the absorbing components in different AGNs, but also because pressure balance is observed (to within the errors) between the components (see 5.4).

An intriguing possibility is that the different components form because of thermal instabilities in the thermal photoionization equilibrium S-curve (Krolik, McKee, & Tarter 1982). This curve marks the points of thermal equilibrium in the  $T, U/T$  plane, where  $T$  is the equilibrium

temperature of the gas, and  $U/T$  is a quantity inversely proportional to the pressure of the gas (see Fig. 15). The wiggles in the S-curve are due to changing heating and cooling rates, as different ions become dominant. The shape of this curve is also affected by the ionizing SED and the metallicity of the absorbing gas (e.g. Komossa & Fink 1997). The high temperature branch lies where only Compton heating is important. Gas in regions of the curve with negative derivative is unstable because any isobaric perturbation will be amplified, leading to net cooling or heating. Then, the different components observed form simply, when the gas is driven to the stable (positive slope) branches of the curve, while tending toward equilibrium.

#### 5.4. Pressure Balance between the Absorbing Components

Krongold et al. (2003) reported that the two components in the ionized absorber of NGC 3783 are in pressure balance to within 7%, which suggested that the absorption could arise from two phases of the same medium. As we shall point here, this also seems to be the situation for the ionized absorber of NGC 985.

As can be observed in Figure 15a, the HIP and the LIP in the best fit model of the NGC 985 *Chandra* data have very different equilibrium temperatures but lie close to each other in the  $U/T$  axis. As mentioned before, with the adopted definition of the ionization parameter ( $U$ ), this ratio is inversely proportional to  $P$ , the gas pressure. Hence, assuming that the HIP and the LIP have the same location, the gas pressure between them is indistin-

guishable within 25%, (the pressure of the phases is consistent with a single value at a level well within  $2\sigma$ ).

We stress again the fact that the absorbing material does not span all the points in the stable branches of the S-curve, but rather it is concentrated in separate phases (see §2.2). Therefore, although the effect of thermal instabilities may be partially responsible for the formation of the phases (§5.3), this cannot alone explain the observations. One possibility is that these phases form as the gas tends to go to the stable branches of the thermal equilibrium curve, but keeping pressure balance between them (see below).

There are two special considerations regarding the validity of the pressure equilibrium result that have to be discussed at this point:

(1) The shape of the SED: Kaspi et al. (2001) and Steenbrugge et al. (2003) have shown that the shape of the SED in the far UV (the unobservable region of the spectrum) has a negligible effect on the charge states absorbing in the X-ray region. However, the curve of thermal equilibrium does depend on the shape of the SED at these wavelengths. Thus, it is possible that SEDs with a UV-X ray break different to the one assumed here would result in two phases lying out of pressure balance. In other words, our result could be reflecting specific characteristics of our chosen SED. To further investigate this possibility, we have repeated our entire analysis with the SED presented in Figure 3b (with the UV-X ray break at 1 keV instead of 0.1 keV). This choice gives the maximum effect introduced in our results by SED uncertainties since the break cannot be at larger

energies because then, the observed spectrum would be directly affected. We find that pressure equilibrium is found regardless of the assumed shape of the far UV SED (see Figure 15b).

(2) The analysis of the LIP is based mostly on the UTA: As discussed in §2.2.1, the lack of reliable DRR for low Fe charge states may be producing an underestimate of the ionization parameter of the LIP. Even if this effect is real, it does not modify the analysis presented here in any way. More accurate DR rates would shift the position of the LIP to higher values of both pressure and temperature in the S-curve ( $\Delta \log U < +0.3$ , see §2.2.1). However, the shift is insufficient to move the LIP out of pressure equilibrium with the HIP. On the contrary, such a change would make the pressure of both components even more closely matched (Figure 15).

## 5.5. Pressure Confinement of the Absorbing Components

A striking result is that pressure equilibrium between the two phases is also found in the BeppoSAX observation of NGC 985. This can be observed in Figure 16, where the S-curve for the SED used in the BeppoSAX analysis is shown, and the positions of the HIP and the LIP in this model are also marked. Although it is not clear what drives the change of ionization in the HIP, both phases again align close to a single value of  $\log U/T$ , as would be expected if one of the two components confines the other one (or as if both components are pressure confined by a third phase).

There are two necessary conditions for this to happen: (1) The hydrodynamic timescale ( $t_H$ ) in the confined medium has

to be shorter than the timescale in which the gas reacts to the changes of the continuum. The sound velocity  $v_s$  for media at temperature  $\lesssim 10^6$  K is  $\lesssim 100$  km s $^{-1}$ , and the hydrodynamic timescale can be estimated as  $t_H \geq \Delta R/v_s$ , where  $\Delta R$  is the scale size of the medium. For a single gas cloud with conditions typical of ionized absorbers ( $10^4$  K  $< T < 10^6$  K, and  $N_H >$  few  $10^{21}$  cm $^{-2}$ ), the hydrodynamic timescale will always be larger than the photoionization timescale, which prevents the gas pressure from responding to the change in the incident continuum quickly enough to remain in pressure equilibrium. This is true for any density inferred using the ionization parameters from our model, assuming that the gas is located anywhere within 10 parsecs of the central source. Thus, an important conclusion is that the phases can only be in true pressure balance if the confined medium is composed by a large number of small clouds ( $\sim 10^4$  clouds), so that the hydrodynamic time scale can be shorter than the photoionization timescale. The total column density of the absorber would result from the individual contributions of the clouds.

(2) The photoionization equilibrium timescale of the media has to be shorter than the variability timescale of the central source, in order for the absorbing material to be close to photoionization equilibrium. This condition is assumed in our analysis. Clearly, if the gas is out of photoionization equilibrium, then the ionization parameters and temperatures derived here are not meaningful, and the absorbing gas is not even constrained to lie on the S-curve. We note that photoionization equilibrium of the confining medium is not required for

pressure confinement (see §5.5.3).

We will follow the discussion assuming that these two conditions are indeed satisfied (but see 5.6). In such a scenario, the confining medium would be responding to the changes in the continuum, and moving freely on the S-curve. The confined medium, on the other hand, would not be able to move freely in the S-curve, rather it would have to follow at all times the position of the confining medium in the U/T axis. This means that the confined medium would have to adapt to the ionizing continuum with a constrained value of the pressure at all times. Thus, to reach the photoionization equilibrium temperature, the confined phase would have to expand or contract to keep pressure balance with the confining medium. Then, the ionization parameter (and thus, the opacity) of the confined phase would be determined not only by the change in flux of the central source (as in an isolated system), but also by the change in density due to the change in volume.

### 5.5.1. Pressure Confinement of the HIP by the LIP

This scenario can easily explain the observed behavior of the HIP between the BeppoSAX and *Chandra* observations: as the flux drops, the LIP gets colder and its pressure drops. Hence, the HIP would have to expand to decrease its pressure. The drop in density of the HIP would increase its ionization parameter and temperature (even though the flux is dropping), until photoionization equilibrium is reached.

However, an inconsistency for this picture is that the column density of the LIP is smaller than that of the HIP and its den-

sity is larger (if the phases are at the same distance, the difference in U between them should be mostly an effect of the different densities). This would require the HIP to be more extended than the LIP, and at the same time, the HIP would have to be made up of several small clouds immersed in the LIP. We find it extremely unlikely that these two conditions can be satisfied simultaneously.

### 5.5.2. Pressure Confinement of the LIP by the HIP

A second scenario is that the HIP is confining the LIP. However, the HIP would have to be out of photoionization equilibrium, in order to explain the changes in ionization parameter. This picture is not possible, since as explained before, if this phase is not in photoionization equilibrium, then its position on the T-U/T plane is unknown. Thus, the alignment on the S-curve would have to be considered just a bias induced by our analysis (see §5.6).

### 5.5.3. Pressure Confinement of the HIP and the LIP by a Third Component

A third scenario is that a more ionized component is confining both the HIP and the LIP. Being more ionized, this component would require a density lower than that of the HIP (which is already 30 times smaller than the density of the LIP). In this case we have two possibilities. The first is that despite the low density, this component still has time to adapt to the changes in the continuum, and therefore is in photoionization equilibrium. The second is that this is not the case. In either scenario, the HIP and the LIP would have

to follow the position of this hypothesized phase in the  $U/T$  axis. In the photoionization equilibrium situation the third component has to be located on the curve of thermal stability. In the non-photoionization equilibrium case, the component could be located off the curve, as long as the pressure imposed by this phase on the other two is compatible with the region of the S curve where multiple phases can survive, otherwise the phases would dissolve.

This scenario is appealing because the presence of this phase could easily explain the observed change of ionization parameter of both the LIP and the HIP, between the BeppoSAX and *Chandra* observations, as we show below. In addition, the data hints the presence of more ionized gas (see Fig. 11). In NGC 3783, the presence of such absorber has already been established, and found to be in pressure balance with the less ionized components (Netzer et al. 2003), which further suggests that this could be the case in NGC 985. Evidently, much better data and time evolving photoionization models (e.g. Nicastro et al. 1999) are needed to explore further this scenario.

If a third confining component is the correct picture, then the HIP and the LIP have to be close to photoionization equilibrium, but may not respond “as expected” to the flux variations because their pressure is fixed to the pressure of the hottest phase. If this hot phase does not change its position on the  $(U/T, T)$  plane dramatically in response to continuum changes (because it is out of photoionization equilibrium or because the gas lies on a steep part of the S-curve), then the HIP and/or the LIP may appear as if they were not

following (or not even responding to) the continuum.

## 5.6. The Absorbing Components Are Not in Pressure Balance

From the last sections, it is clear that a scenario of pressure-confining is appealing because, due to the regions of thermal stability in the S-curve, it can explain the different absorption components observed in the spectra of Seyfert galaxies. However, such scenario also imposes strong physical conditions on the media that could be difficult to satisfy. There is not enough evidence currently to rule out or confirm such a scenario and other possibilities have to be considered.

If the pressure confinement is not real, why do the phases align close to a single value of  $U/T$ ? The answer to this question may rely on the shape of the S-curve. For several SEDs, the S-curve can be extremely steep in a large range of temperatures (between  $10^4$  to  $10^6$  K) where photoionized gas absorbs in the X-ray range (Krolik & Kriss 2001). Large gradients of temperature (factors 10-50) can then arise from small changes of the gas pressure. This is clearly illustrated in Figures 15 and 16. Thus, if several absorbing components were in photoionization equilibrium and located in the “vertical region” of the S-curve, but were completely disconnected from each other, they would appear as if they were in pressure balance. While this is certainly plausible, we note that there are also SEDs that do not show such a pronounced vertical branch (Komossa & Fink 1997). In those cases, it is possible to disentangle true pressure balance from appar-

ent pressure balance (see for example the S-curve obtained for the SED derived by Krongold et al. 2003 in their analysis of NGC 3783, their Fig. 16). Thus, discriminating true pressure balance from apparent pressure balance strongly depends on (1) the quality of the X-ray spectrum to constrain better the position of the phases in the (T,U/T) plane, and (2) the true shape of the SED, which is, however, always uncertain.

Evidently, if the gas is out of photoionization equilibrium, the curves of thermal stability discussed here are not relevant to describing the physical state of the gas. Then, we would not know if the phases are or are not in pressure balance. We note that the excellent fits obtained for the high quality data of NGC 3783 (Krongold et al. 2003, Netzer et al. 2003) suggest that the gas is at least close to photoionization equilibrium. Time evolving photoionization models applied to high quality data are the best way to determine if the data are in photoionization equilibrium, and to further study possible scenarios of pressure confinement out of equilibrium.

Additional complexity is present because the X-ray detectors are most sensitive to absorption features produced by gas in exactly the vertical region of the S-curve. So, the detection of components only in the vertical branch (i.e. in apparent pressure equilibrium) could be the reflection of an observational bias. To explore this possibility we have simulated a series of *Chandra* observations using the same exposure time and the same best continuum model for the NGC 985 observation (see Table 2). We have simulated data with two different absorption scenarios:

- (1) The first dataset was produced using the HIP plus gas less ionized than the LIP (i.e. gas located to the left of the LIP in the horizontal branch of the S-curve with  $\log U = -0.8$  and  $\log N_H = 21.5$  [ $\text{cm}^{-2}$ ]). We modeled these data with PHASE and found that the presence of colder gas was easily detected and constrained.
- (2) The second dataset was simulated using 3 absorption components: the HIP and the LIP (Table 3), plus a third cooler absorber with relatively large column density ( $\log U = -0.8$  and  $\log N_H = 21.5$  [ $\text{cm}^{-2}$ ]). First, we modeled these data including only two absorption components. This approach gives an acceptable fit, but the ionization parameter and column density of the low ionization gas are only upper limits, which allows the presence of the additional cold ionized material. Then, we fitted the simulated data with three absorbing components. With this model the values of the column density and ionization parameter of the LIP can be recovered within a significance of  $\approx 1.5\sigma$ , as observed in Figure 17a, and the parameters of the HIP can also be recovered within a level  $\approx 1\sigma$ . The third component is well constrained in  $N_H$  ( $21.4 < N_H < 21.6$ ), but the model is consistent with the actual values used to simulate this gas at a significance level of only  $\approx 2.5\sigma$ , with  $U$  poorly constrained (to a factor 100). This can be observed in Figure 17b, where we present the confidence region for this component. In fact, our simulations show that the presence of gas 75 times less ionized than the LIP ( $\log U \sim -2$ ) would still be detectable, because the bound-free opacity increases dramatically with decreasing  $U$ . However, the ionization state of such gas

would be basically unconstrained ( $\log U < -0.5$ ). Thus, even with low S/N ratio data, we feel confident that there is no additional absorbing material along the horizontal branch of the S-curve (i.e. gas out of pressure balance) in the spectrum of NGC 985, or it would be detected. Evidently, the high quality data of NGC 3783 is less susceptible to this kind of bias.

All these tests indicate that, while the pressure-confining scenario might be appropriate, it requires fragmentation of the confined absorber, and thus, the idea should be tested even further. Any model of the ionized absorbers around AGN has to explain several points: (1) Why is there not a significant amount of gas on the horizontal branch of the S-curve, at temperatures lower than the one of the LIP? (2) Why does the gas tend to give preference to special values of the ionization parameter? (3) How do the observed components relate to the stable branches of the S-curve, assuming that the gas is indeed in photoionization equilibrium? (4) What is the relation between the UV and the X-ray absorbers? In several objects, the observed X-ray absorbing components do not occupy all the points in the stable branches of the S-curve, and the absorption seems to be produced from similar charge states. A simple model with absorbing components located at random cannot explain these properties. Rather they seem to point to real properties of the structure of active nuclei.

A perhaps more basic question that still has to be answered is ‘where are the X-ray absorbers located?’ Are they located at large scale distances (parsecs from the nucleus; Netzer et al. 2003; Behar et al.

2003) forming part of the biconical flow observed for the narrow emission line regions (Kinkhabwala et al. 2002; Behar et al. 2003)? Or, on the contrary, are they closer (at subparsec distances, e.g. Nicasastro et al. 1999; Netzer et al. 2002; Gabel et al. 2003; Reeves et al. 2003) and part of a disk wind (Elvis 2000)?

Answers to these questions will help us understand what is the genesis of these winds and what is their relation to the black hole and the accretion disk.

## 6. ALTERNATIVE SCENARIOS FOR THE IONIZATION MECHANISM

The solution found for the ionized absorber through photoionization models is satisfactory and carries important implications for the nuclear environment of AGNs. Nevertheless, an alternative to photoionization by the central source deserves to be explored for the HIP, since this phase does not respond simply to continuum changes.

The ring located in NGC 985 at a distance of kiloparsecs from the nucleus has a large inclination angle, which brings the possibility that our line of sight to the central source crosses through collisionally ionized material in this ring. Such collisions would be produced by an expanding wave triggered by a pole-on merger (see for instance Karovska et al. 2002 for Centaurus A). Hence, there is a chance that the material producing the absorption observed in X-rays is collisionally ionized (the HIP is too hot to be photoionized by the starburst induced by the merger). If collisions drive the ionization, the temperature of the HIP is at least an order of magnitude hotter than our estimate, and thus

the two components cannot be in pressure equilibrium. Although this scenario cannot be excluded, we notice that the change in ionization structure of the HIP observed in the 3 year period elapsed between the observations, requires an increase in the electron temperature by at least a factor of 2 in the HIP (the temperature variation is significant at a level  $2.6\sigma$ ), which suggests that this gas is probably not ionized by collisional mechanisms. Furthermore, if the absorption of the HIP arises in the ring, then the pressure balance found between the phases would have to be interpreted as a pure coincidence. We stress again that pressure balance is also observed in NGC 3783, a relatively undisturbed galaxy.

## 7. SUMMARY

A new *Chandra* observation and an archival BeppoSAX observation are used to study the nuclear environment of NGC 985. Absorption features consistent with the presence of ionized gas in the nuclear environment of this Seyfert 1 galaxy are detected in both datasets. We have used the code PHASE (Krongold et al. 2003) to model in a self-consistent way the ionized absorber, and to further study possible changes in the opacity of the gas to continuum variability. Our main results are as follows:

(1) The intrinsic continuum of the source is well reproduced by a power law ( $\Gamma \approx 1.4 - 1.6$ ) and a thermal component ( $kT=0.1$  keV). This continuum was attenuated by an equivalent hydrogen column density of  $3.0 \times 10^{20}$  cm $^{-2}$  to account for Galactic absorption.

(2) The data requires two absorption components different by a factor of 29 in

ionization parameter, and by a factor of 3 in H column density. The hotter phase is clearly identified through broad absorption features produced by several blends of Fe L-shell absorption, and the cooler component is detected due to the presence of a deep Fe M-shell UTA. However, the signal to noise ratio of the *Chandra* data does not allow the identification of significant ( $\sigma > 2$ ) narrow (unblended) absorption features. This results in a poor determination of the outflow velocities of the components ( $581 \pm 206$  km s $^{-1}$  for the high ionization phase and  $197 \pm 184$  km s $^{-1}$  for the low ionization one).

(3) Despite the limited signal to noise ratio of the *Chandra* data, the ionization state of both components is well constrained thanks to several features of Fe L-shell absorption, but mainly because of the Fe UTA. The lack of accurate dielectronic recombination rates of low charge states of Fe (Netzer et al. 2003) introduces an uncertainty by a factor less than 2 in the ionization parameter of the phases; however, our results are robust and highly insensitive to this source of error.

(4) The outflow velocity of both components is consistent with most of the absorption components found in the UV spectrum of this object. In particular, both components are consistent with the UV component with outflow velocity of 404 km s $^{-1}$ , which is hot enough to absorb in the X-ray regime (Arav 2002). In addition, the low ionization component in the X-rays produces significant amounts of O VI, N V, and C IV, which strongly suggests that the absorption features in both bands are the manifestation of a single wind.

(5) The data set tight limits on the pres-

ence of additional cold absorption components, showing that gas with temperature  $< 10^6$  K clumps around the two absorbers detected. On the other hand, the presence of a third component, hotter than the other two ( $T > 10^6$  K), and producing Fe K-shell absorption, is hinted by the data. However, data with better signal to noise ratio is needed to constrain the properties of such component.

(6) The gas detected in the spectrum of NGC 985 has strikingly similar characteristics to the gas found in NGC 3783 and IRAS 13349+2438: (1) absorption produced by cold gas (Fe VII-XIII), (2) absorption by hot gas, dominated by Fe XVII-XXII, and (3) no significant absorption consistent with Fe XIV-XVI. Then a continuous range of ionization parameters is disfavored (at least in these objects). These similar characteristics further suggest that this is an intrinsic property of the absorbers, probably related to the unstable branches of the thermal equilibrium curve.

(7) The X-ray luminosity drops by a factor 2.3 between the BeppoSAX and *Chandra* observations (separated by  $\sim 3$  years). We detect (model dependent) variability in the opacity of the absorbers. While the colder component is consistent with a simple picture of photoionization equilibrium, the ionization state of the hotter component seems to increase while the flux drops.

(8) The most striking result in our analysis is that the two absorbing phases are consistent (to within the errors) with pressure equilibrium. This result is obtained during both the *Chandra* and the BeppoSAX observations. Based on this, we speculate that the absorption arises from a multi-phase wind. Such a scenario can ex-

plain the change in opacity of both components during the observations, but requires that a third hotter component is pressure-confining the two phases. Thus, our analysis strongly points to a 3-phase medium, just like the wind suggested in NGC 3783.

(9) An important implication of our analysis is that, if the pressure-confining scenario is real, then fragmentation of the confined phases in a large number of clouds is required.

The analysis presented in this paper provides further evidence that warm absorbers in AGN are simple systems that can be relatively well understood. The high resolution spectroscopic capabilities of the new generation of X-ray observatories have revealed warm absorbers as strong winds, now recognized as an important feature of AGN structure. Here, we have used high and low resolution data to constrain and characterize the physical conditions and structure of these winds. Measuring the response in the opacity to variability of the ionizing flux, we suggest that the nature of the ionized absorber is that of a multi-phase wind, with one phase confining the other two. The implications of this result are extremely important to our understanding of quasar energy budgets, as well as to our understanding of the interaction between these winds and the interstellar medium of the host galaxy. However, our analysis is based on a comparison between high and low resolution data. Only a direct comparison between high resolution data will allow further testing of the scenario presented here, leading to a deeper understanding of the nature of AGN and quasars.

We thank the anonymous referee for valuable comments that helped improve our work. This research has been partly supported by NASA Contract NAS8-39073 (Chandra X-ray Center), NASA grant NAS G02-3122A, and Chandra General Observer Program TM3-4006A. This research has made use of the NASA/IPAC Extragalactic Database (NED) which is operated by the Jet Propulsion Laboratory, California Institute of Technology, under contract with the National Aeronautics and Space Administration.

TABLE 1  
OBSERVATION LOG OF NGC 985

Observatory	Sequence Number	UT Start	Exp Time (ks) <sup>a</sup>
BeppoSAX	50862001	1999 AUG 20 06:38	95.0
<i>Chandra</i>	700449	2002 JUN 24 19:33	77.7

<sup>a</sup>Sum of good time intervals.

TABLE 2  
CONTINUUM PARAMETERS

Parameter	Chandra Data		BeppoSAX Data
	0.7-8 keV <sup>a</sup>	3-8 keV	0.1-110 keV <sup>a</sup>
$\Gamma^b$	1.60±0.03	1.62±0.02	1.40±.04
Norm <sup>c</sup>	1.22±0.04	1.22±0.04	2.47±0.04
BB kT <sup>d</sup>	0.10±0.01	...	0.10±0.02
Norm <sup>e</sup>	3.7±0.8	...	8.8±1.2
$E_c$ (keV) <sup>f</sup>	...	...	67 ± 24
Flux(.1-2keV) <sup>g</sup>	0.63±0.12	...	1.34±0.08
Flux(2-10keV) <sup>g</sup>	0.54±0.09	...	1.49±0.12
R <sup>h</sup>	...	...	0.0+0.35
$\chi^2/d.o.f.$	179.0/174	46.7/49	116.4/110

<sup>a</sup>Continuum fits carried out with the self-consistent inclusion of an ionized absorber. See Tables 3 and 4.

<sup>b</sup>Power Law Photon Index

<sup>c</sup>Power law normalization in  $10^{-3}$  photons  $\text{keV}^{-1} \text{ cm}^{-2} \text{ s}^{-1}$  at 1 keV

<sup>d</sup>Blackbody Temperature in keV

<sup>e</sup>Blackbody Normalization in  $10^{-5} L_{39}/D_{10}^2$ , where  $L_{39}$  is the source luminosity in units of  $10^{39} \text{ erg s}^{-1}$  and  $D_{10}$  is the distance to the source in units of 10 kpc

<sup>f</sup>High Energy Cutoff as inferred from the SAX data

<sup>g</sup>In units of  $10^{-11} \text{ ergs cm}^{-2} \text{ s}^{-1}$

<sup>h</sup>Reflection component factor ( $R = \Delta\Omega/2\pi$ , with  $\Delta\Omega$  the solid angle subtended by the reflector).

TABLE 3  
TWO PHASE ABSORBER PARAMETERS FOR *Chandra* DATA

Parameter	High-Ionization HIP	Low-Ionization LIP
Log U <sup>a</sup>	1.34±0.10	-0.12 <sup>+0.30</sup> <sub>-0.09</sub>
Log N <sub>H</sub> (cm <sup>-2</sup> ) <sup>a</sup>	21.81±.22	21.39±0.19
V <sub>Turb</sub> (km s <sup>-1</sup> ) <sup>b</sup>	350	350
V <sub>Out</sub> (km s <sup>-1</sup> ) <sup>a</sup>	581±206	197±184
[Log T (K)] <sup>c</sup>	5.79±0.11	4.47±0.04
Log U/T ( $\propto 1/P^d$ )	-4.45 ±0.21	-4.59 <sup>+0.30</sup> <sub>-0.13</sub>
Log U <sub>x</sub> <sup>e</sup>	-1.09±0.10	-2.55±0.09

<sup>a</sup>Free parameters of the model.

<sup>b</sup>Fixed parameter.

<sup>c</sup>Derived from the column density and ionization parameter, assuming photoionization equilibrium.

<sup>d</sup>The gas pressure  $P \propto n_e T$ . Assuming that both phases lie at the same distance from the central source  $n_e \propto 1/U$ , and  $P \propto T/U$ .

<sup>e</sup>Ionization parameter defined in the 0.1-10 keV range (Netzer 1996).

TABLE 4  
TWO PHASE ABSORBER PARAMETERS FOR BEPPoSAX DATA

Parameter	High-Ionization HIP	Low-Ionization LIP
Log U <sup>a</sup>	0.83±0.13	-0.22 <sup>+0.30</sup> <sub>-0.10</sub>
Log N <sub>H</sub> (cm <sup>-2</sup> ) <sup>b</sup>	21.81	21.39
V <sub>Turb</sub> (km s <sup>-1</sup> ) <sup>b</sup>	350	350
V <sub>Out</sub> (km s <sup>-1</sup> ) <sup>b</sup>	581	197
[Log T (K)] <sup>c</sup>	5.48±0.12	4.56±0.05
Log U/T ( $\propto 1/P^d$ )	-4.65 ±0.25	-4.78 <sup>+0.30</sup> <sub>-0.15</sub>
Log U <sub>x</sub> <sup>e</sup>	-1.25±0.13	-2.30±0.10

<sup>a</sup>Free parameter of the model.

<sup>b</sup>Fixed parameters, assuming N<sub>H</sub>, FWHM, and V<sub>Out</sub> values from the best fitting *Chandra* model.

<sup>c</sup>Derived from the column density and ionization parameter, assuming photoionization equilibrium.

<sup>d</sup>The gas pressure P $\propto$ n<sub>e</sub>T. Assuming that both phases lie at the same distance from the central source n<sub>e</sub> $\propto$ 1/U, and P $\propto$ T/U.

<sup>e</sup>Ionization parameter defined in the 0.1-10 keV range (Netzer 1996).

TABLE 5  
IONIC COLUMN DENSITIES<sup>a</sup> PREDICTED BY THE MODELS

HIP			LIP		
Ion	<i>Chandra</i>	BeppoSAX	Ion	<i>Chandra</i>	BeppoSAX
C VI	16.53	16.88	C V	17.31	17.01
C VII	18.34	18.36	C VI	17.64	17.68
N VII	16.46	16.80	N VI	17.03	16.94
N VIII	17.76	17.73	N VII	16.95	16.97
O VII	16.18	16.94	O VII	18.03	18.07
O VIII	17.75	18.09	O VIII	17.48	17.69
O IX	18.61	18.54	Ne VI	17.16	16.97
Ne IX	16.52	17.09	Ne VII	16.70	16.77
Ne X	17.38	17.54	Ne VIII	16.44	16.75
Ne XI	17.66	17.45	Ne IX	16.20	16.78
Mg XI	16.55	16.99	Mg VIII	16.51	16.21
Mg XII	17.10	17.02	Mg IX	16.54	16.57
Mg XIII	16.91	16.56	Mg X	16.10	16.45
Si XIII	16.96	17.09	Si VIII	16.29	15.76
Si XIV	16.98	16.79	Si IX	16.52	16.34
Si XV	16.47	16.03	Si X	16.37	16.53
Fe XVII	16.16	16.60	Fe IX	16.01	15.28
Fe XVIII	16.69	16.83	Fe X	16.24	15.77
Fe XIX	16.81	16.70	Fe XI	16.34	16.11
Fe XX	16.72	16.36	Fe XII	16.19	16.33
Fe XXI	16.28	15.68	Fe XIII	15.92	16.28

<sup>a</sup>log of column density in cm<sup>-2</sup>

TABLE 6

COLUMN DENSITIES<sup>a</sup> OF LOW IONIZATION LIP IONS FROM THE *Chandra* BEST FIT MODEL.

Ion	SED1 <sup>b</sup>	SED2 <sup>c</sup>
O VI	17.23	17.13
N V	15.67	15.39
C IV	15.82	15.23
H I	15.37	15.33

<sup>a</sup>log of column density  
in cm<sup>-2</sup>

<sup>b</sup>SED presented in Fig.  
3a

<sup>c</sup>SED presented in Fig.  
3b

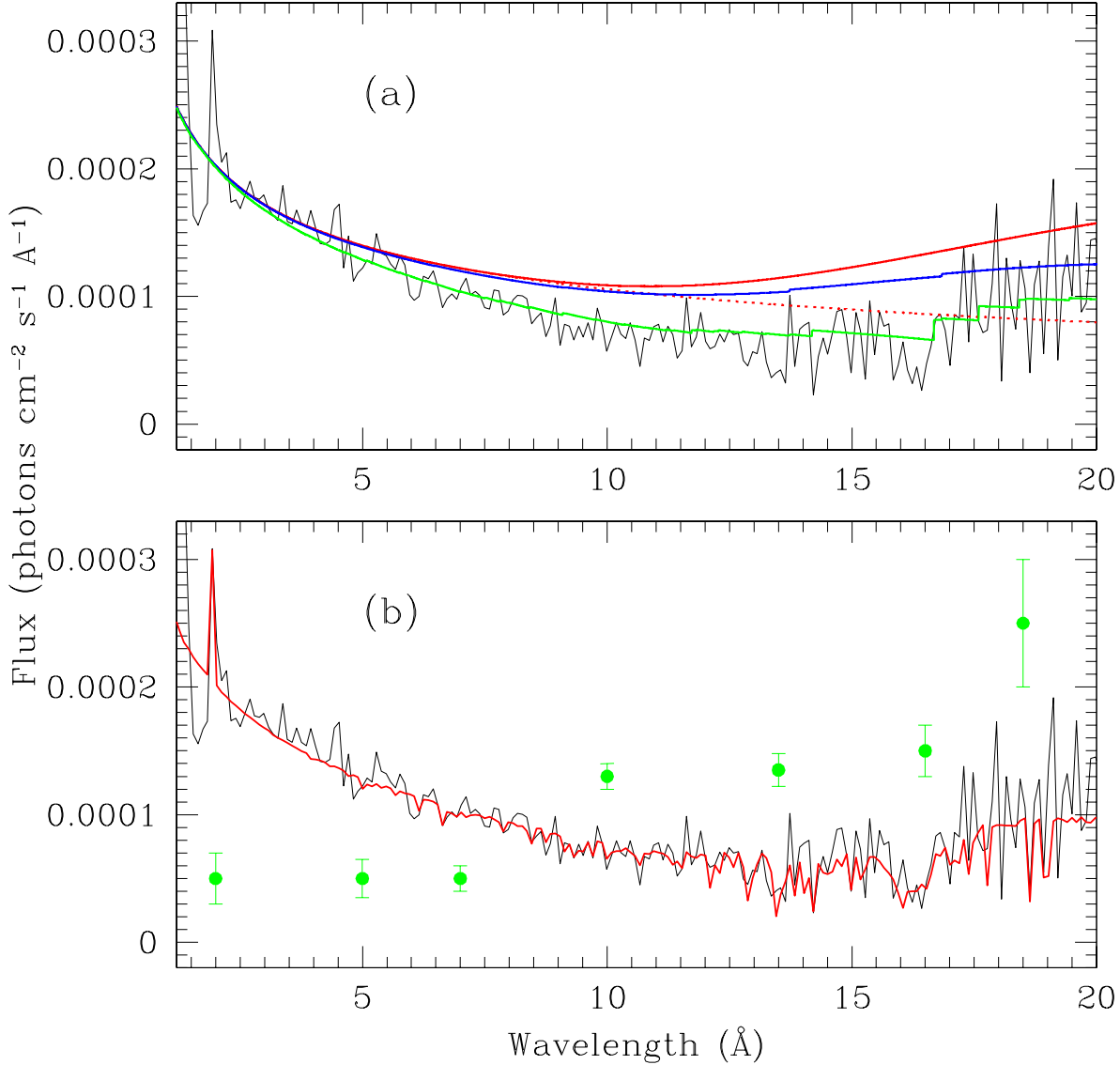


Fig. 1.— Fluxed, combined (MEG+HEG) first-order spectrum of NGC 985. (a) Continuum fitted to the spectrum. The three solid lines stand for (from upper to lower): intrinsic continuum of the source, continuum attenuated by Galactic absorption, and continuum further attenuated by the bound-free photoelectric absorption edges. The dotted line represents the predicted power law without the contribution from the blackbody component. (b) Two phase absorption model plotted for comparison. Typical errors (per bin) are marked with green solid ranges. [See the electronic edition of the Journal for a color version of this figure]

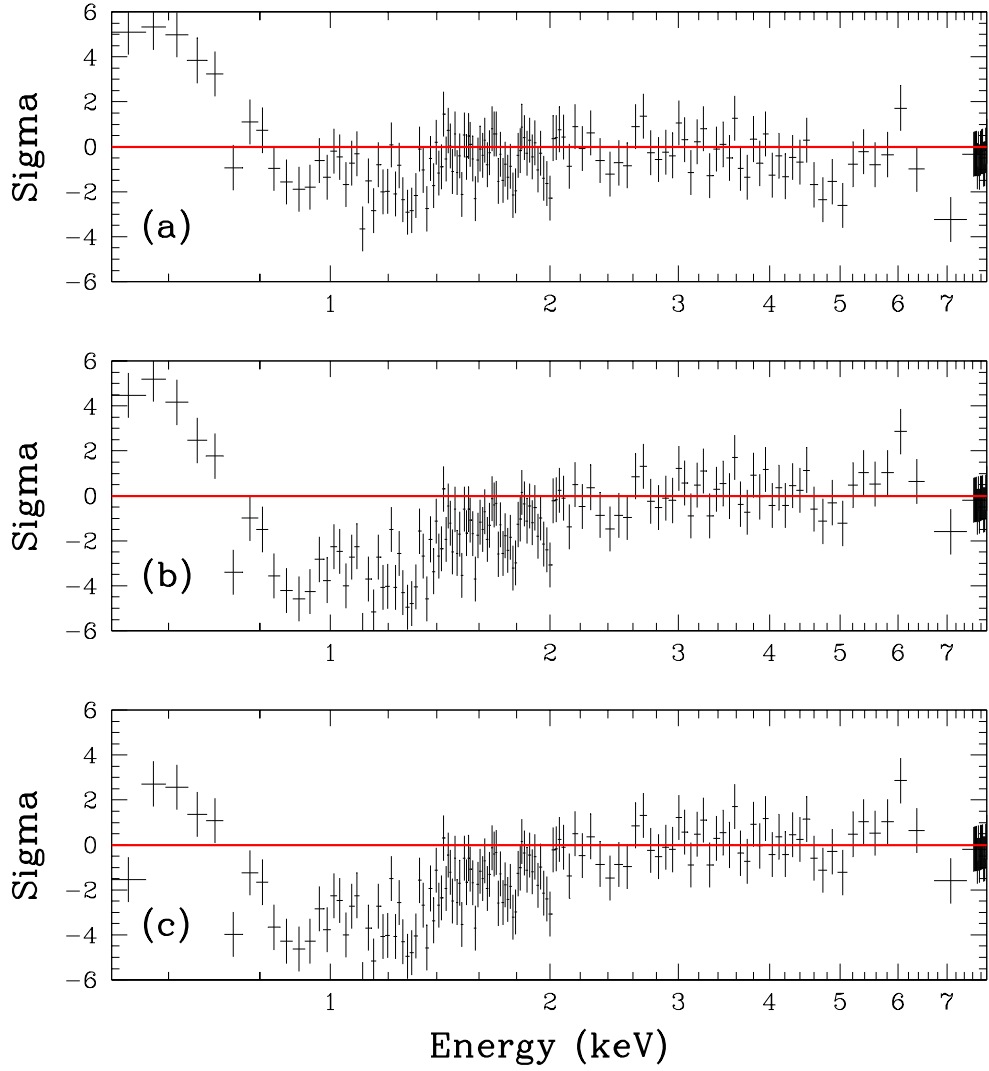


Fig. 2.— Fit residuals for continuum determinations over *Chandra* HEG+MEG data of NGC 985. All models are attenuated by cold gas with  $\log N_H = 20.5$  [cm $^{-2}$ ] due to Galactic absorption. (a) Model including a continuum power law fitted over the entire spectral range (0.6-8keV). (b) Power law fitted only in the 3-8 keV range. (c) Model in Panel (b) plus a soft excess parameterized with a blackbody component. The data are binned to  $> 100$  photons in each channel to make evident the overall features. [See the electronic edition of the Journal for a color version of this figure]

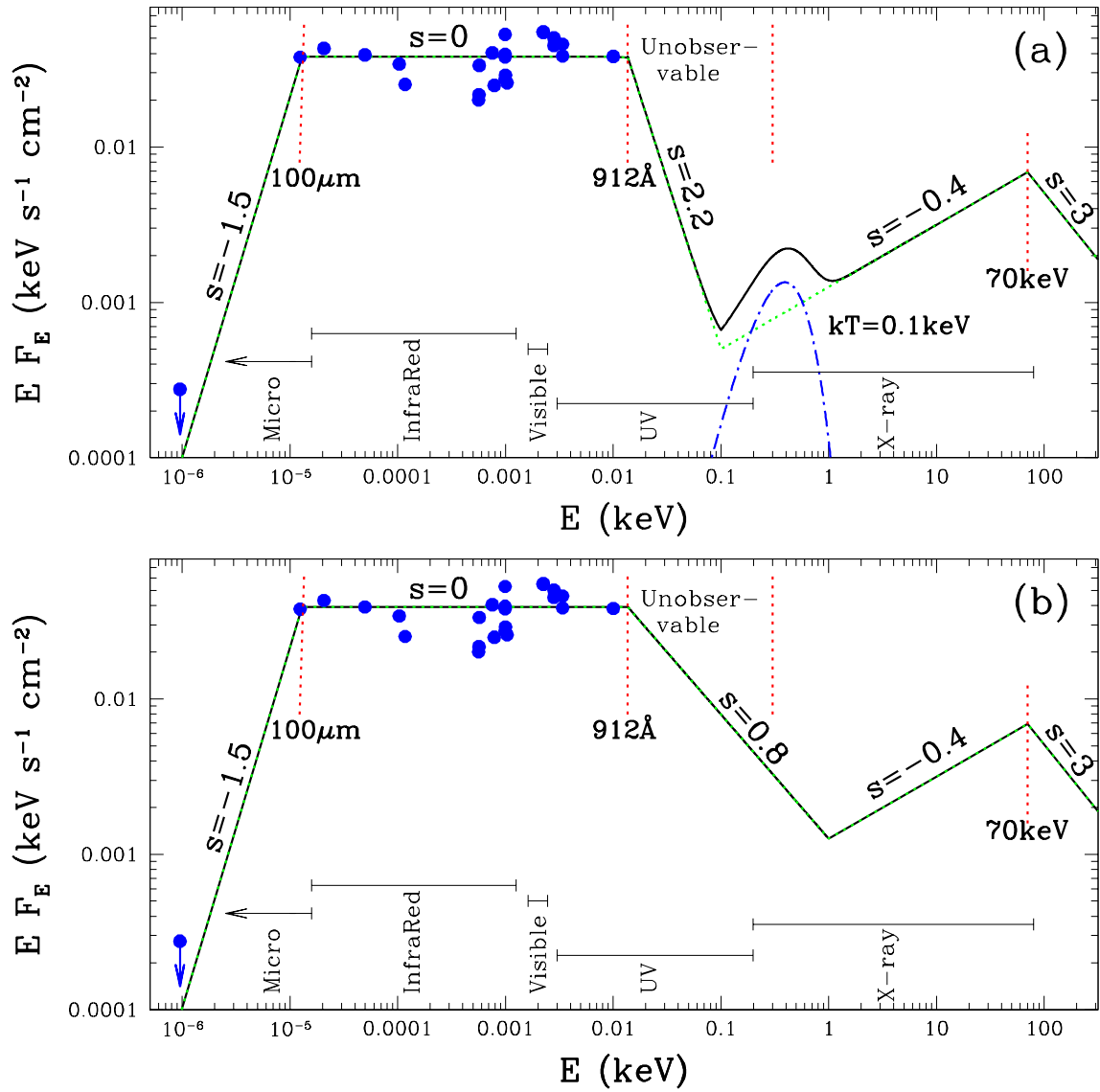


Fig. 3.— Spectral Energy Distribution used to model the ionized absorber in the *Chandra*-HETG data. Filled circles (blue) mark the observed SED of NGC 985 (obtained from NED). The plot shows the slope adopted in each energy range. This slope relates to the photon index as  $\Gamma = s + 2$ . (a) Model with low energy far UV cutoff at 0.1 keV and including the contribution of a blackbody component. (b) Model with high energy far UV cutoff at 1 keV. [See the electronic edition of the Journal for a color version of this figure]

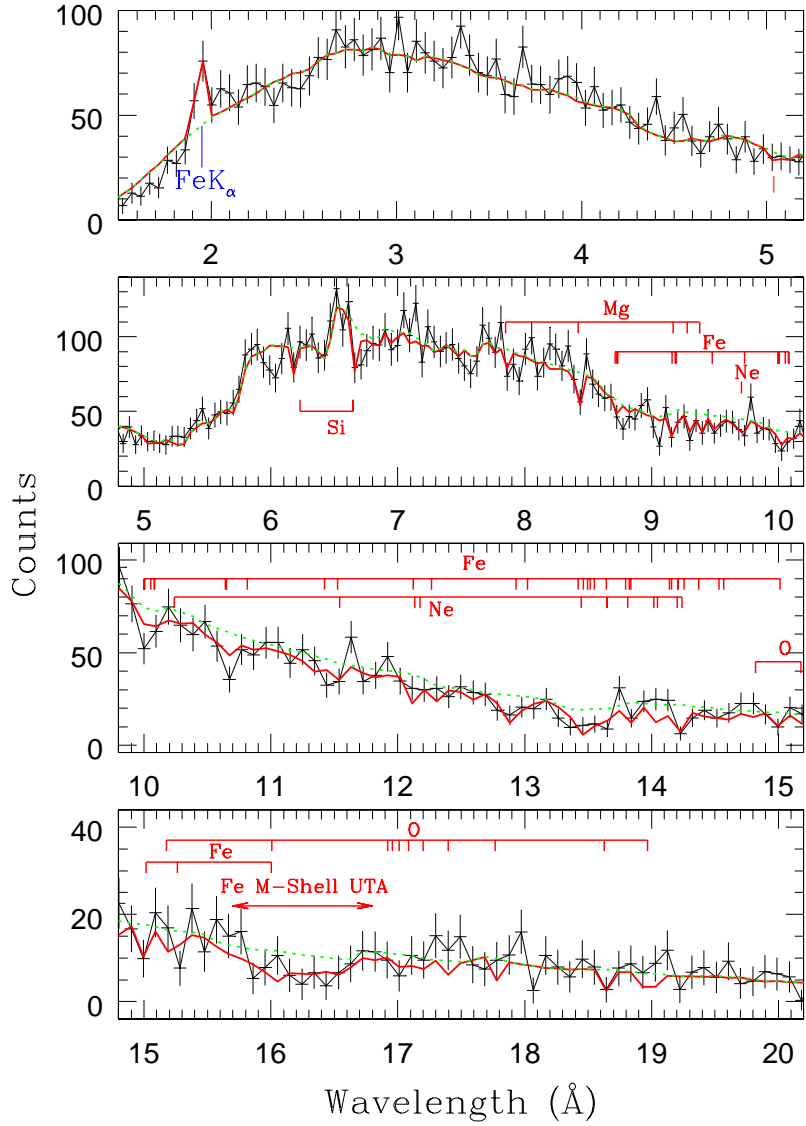


Fig. 4.— Two phase absorber model plotted against the first-order combined MEG+HEG spectrum of NGC 985. Absorption lines predicted are marked along bars at top for each element (red). The continuum level (including edge continuum absorption) is overplotted for comparison (dotted green line). The spectrum is presented in the rest frame system of the absorbing gas. Below 10 Å the data are presented in bins of size 0.05 Å, above 10 Å in bins of size 0.1 Å. [See the electronic edition of the Journal for a color version of this figure]

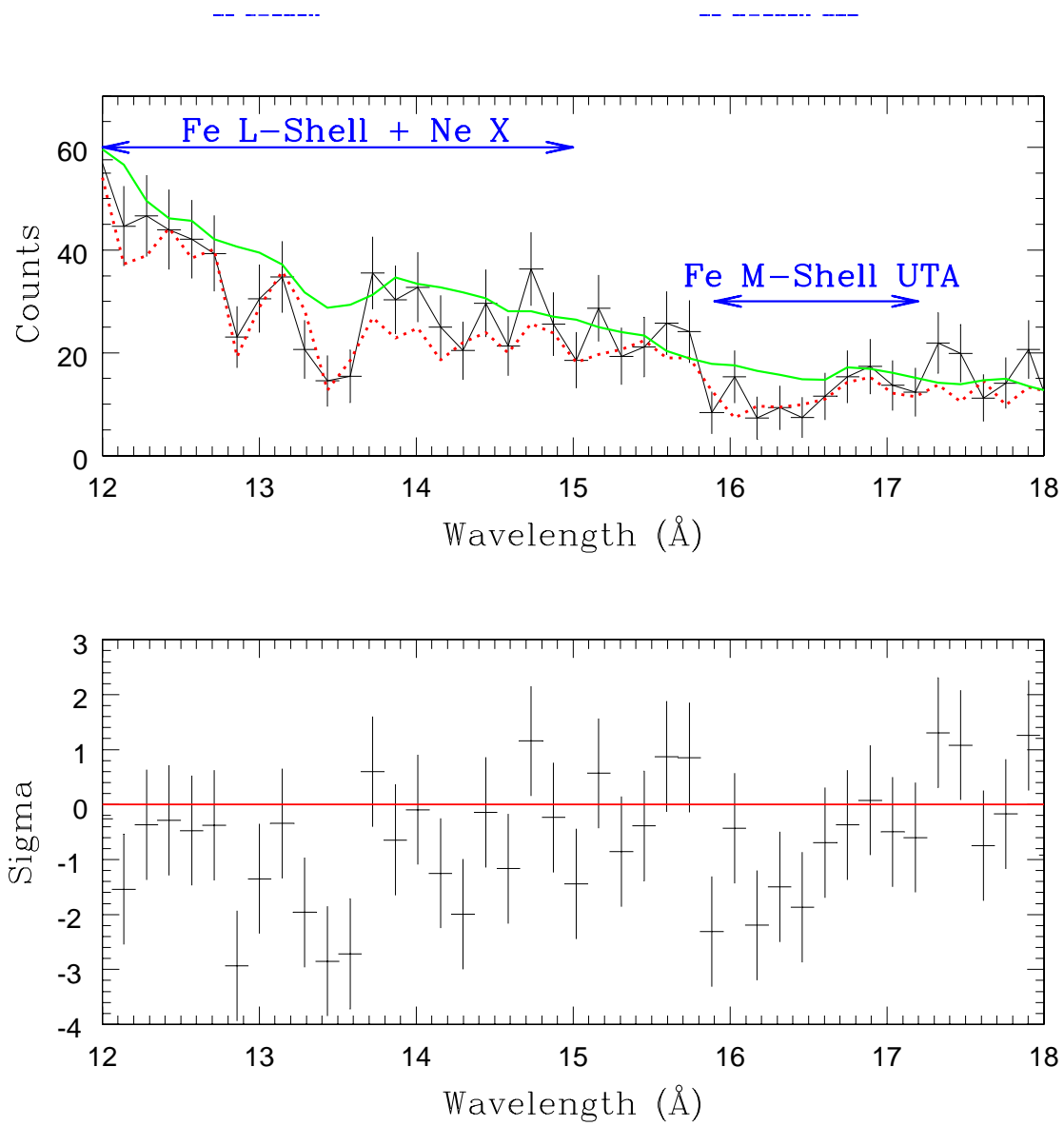


Fig. 5.— Upper panel: MEG+HEG spectrum of NGC 985 grouped in bins of size  $0.15 \text{ \AA}$  (binning factor of 30). The solid line (green) marks the continuum level, including photoelectric bound-free absorption from our model. The final model including resonant absorption is marked with the dotted line (red). The feature in the continuum (solid green line) between  $13.3$  and  $13.8 \text{ \AA}$  is produced by a chip gap in the detector. Lower panel: Residuals (data minus continuum green solid line) in units of standard deviations showing the presence of deep Fe L-shell resonant absorption (significance  $\approx 3\sigma$  per bin) and Fe M-shell inner shell resonant absorption (significance  $\approx 2\sigma$  per bin). [See the electronic edition of the Journal for a color version of this figure]

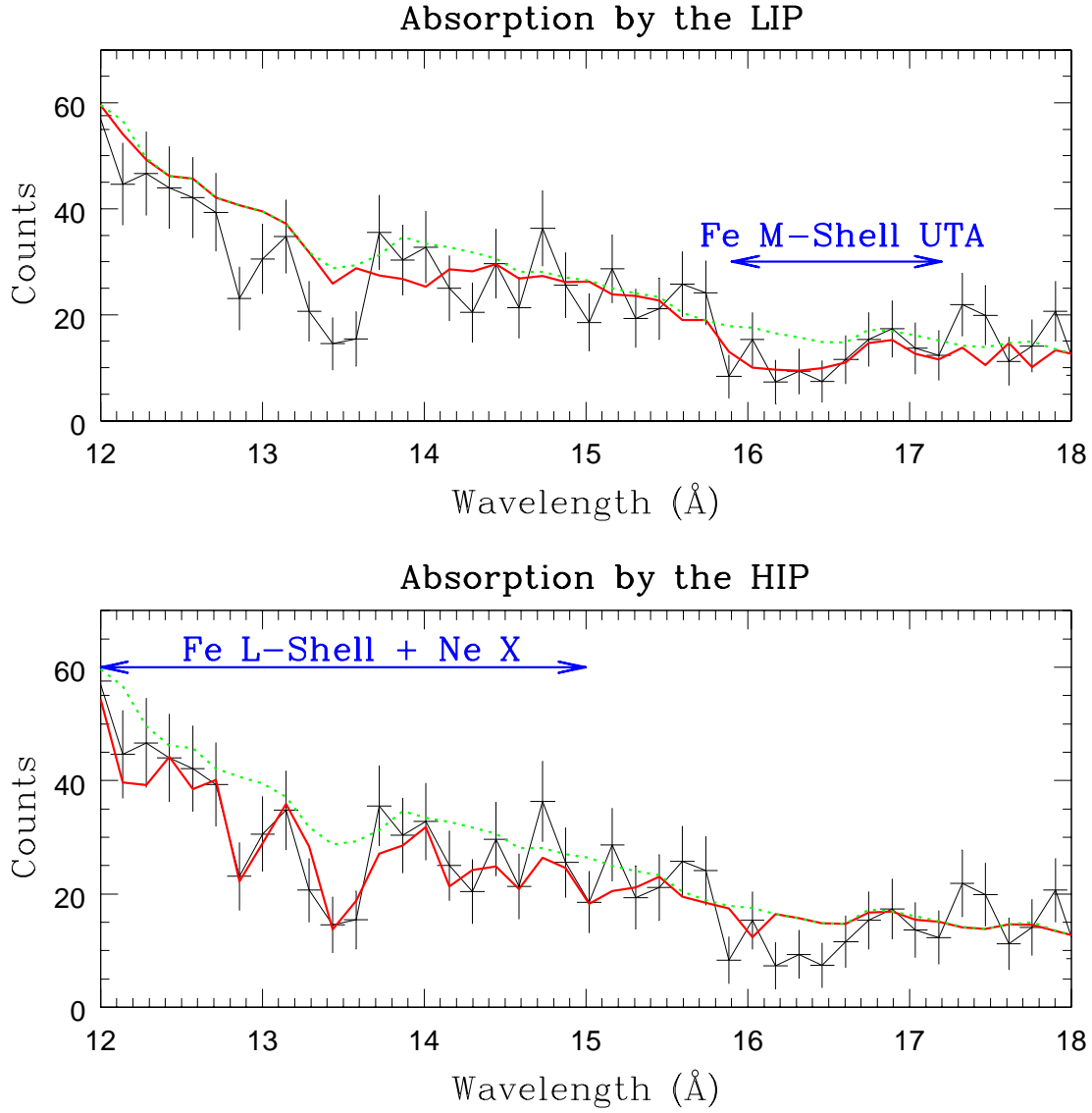


Fig. 6.— Upper Panel: Resonant bound-bound absorption produced by the low ionization phase (LIP) of our model, plotted against the MEG+HEG spectrum of NGC 985 grouped in bins of size  $0.15 \text{ \AA}$  (binning factor of 30). The dotted line (green) marks the continuum level, including bound-free photoelectric absorption from our model. The main feature of this component is the Fe UTA. Lower panel: As upper panel, but showing the contribution from the high ionization phase (HIP). Below  $15 \text{ \AA}$  the spectrum is dominated by Fe L-shell absorption. [See the electronic edition of the Journal for a color version of this figure]

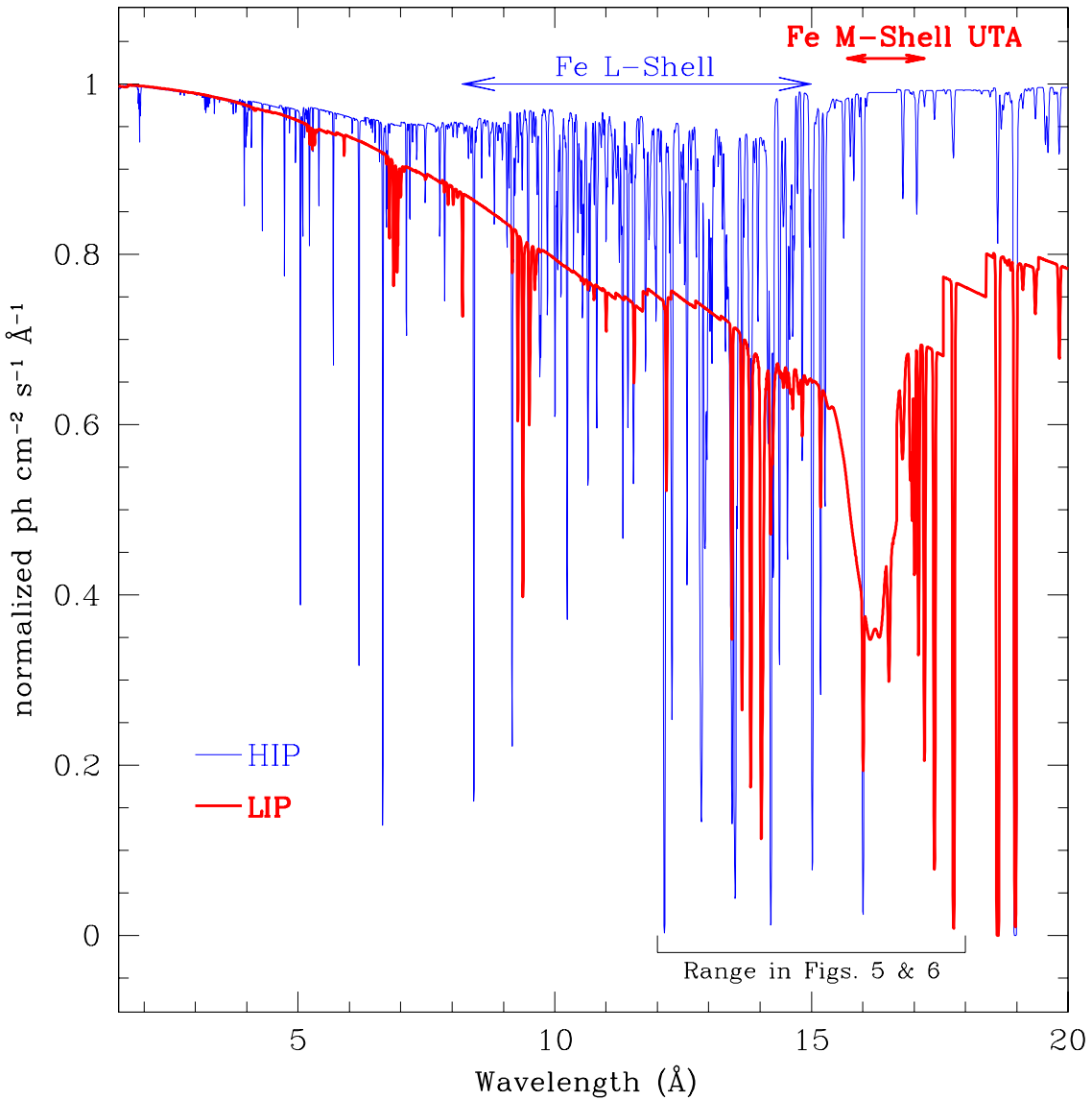


Fig. 7.— Theoretical transmission spectrum of the two absorption components at 0.001 Å resolution. The low ionization component produces most of the bound-free photoelectric absorption and the UTA near 16 Å. The high ionization component produces the Fe L-shell absorption below 15 Å. [See the electronic edition of the Journal for a color version of this figure]

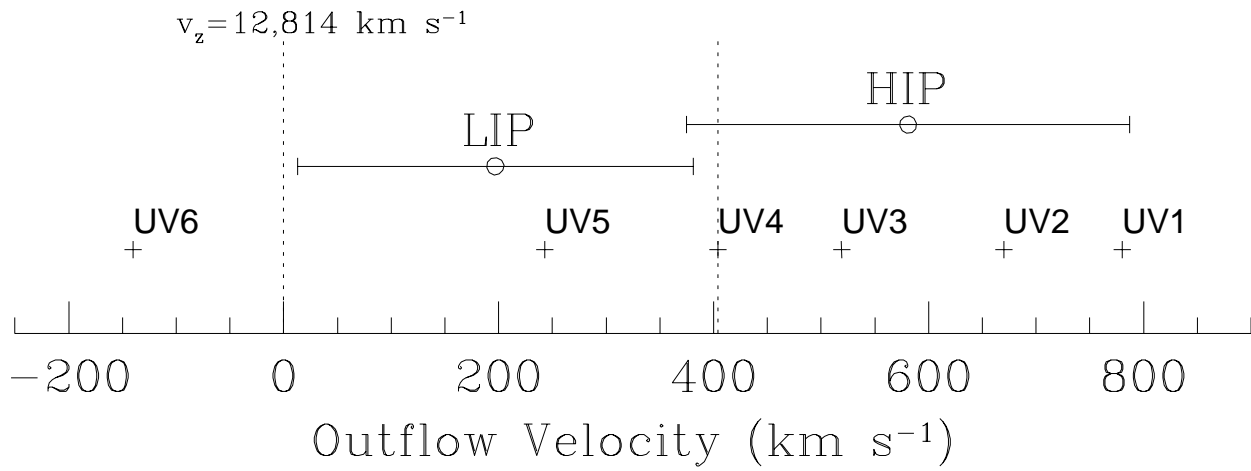


Fig. 8.— Outflow velocities for the HIP and the LIP, and for the 6 absorption components observed in the UV. The HIP is consistent within  $2\sigma$  with UV components 1 to 5, and the LIP with components 3 to 6. Both the HIP and the LIP are consistent with component 4, which was expected to absorb in the X-ray region (Arav 2002).

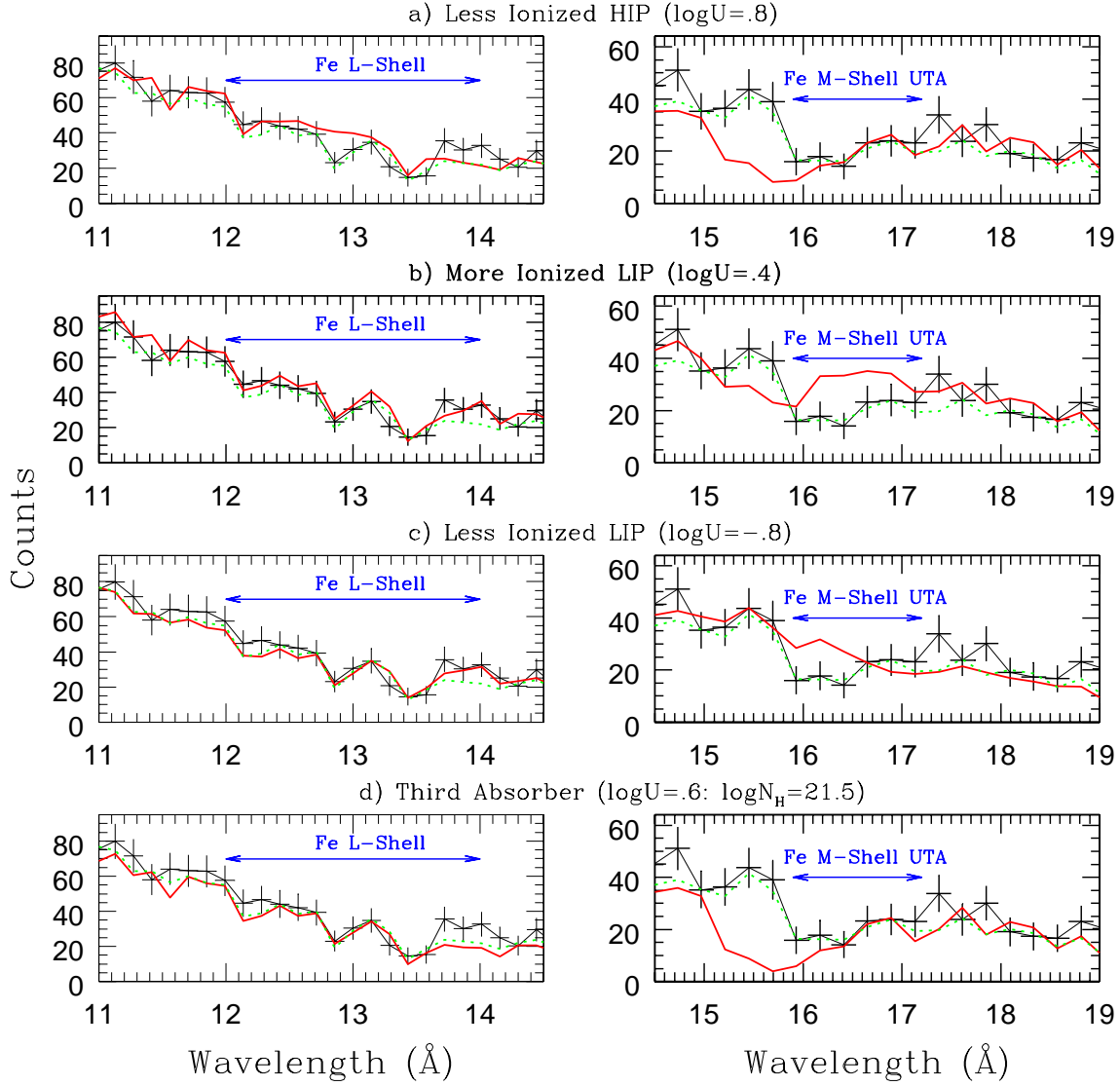


Fig. 9.— Different values for the ionization parameters of our two phase absorber showing inconsistencies with the observed UTA. The left panels present the data in the range 11-14.5 Å in bins of size 0.15 Å (binning factor of 30), the right panels the data in the range 14.5-19 Å in bins of size 0.25 Å (binning factor of 50). The green dotted line shows the best fit model for comparison. Panel (a): Less Ionized HIP,  $\log U=0.8$ . Note that the absorption from Fe L-shell is underestimated. Panel (b): More ionized LIP, the ionization parameter of the low ionization component has been set to  $\log U=0.4$ . Panel (c): Less Ionized LIP,  $\log U=-0.8$ . Panel (d): A third absorber has been included in our model with  $\log U=0.6$  and  $\log N_H=21.5$  [cm $^{-2}$ ]. Including a new component overpredicts the absorption by the UTA, which further suggests that the absorbing gas tends to clump. [See the electronic edition of the Journal for a color version of this figure]

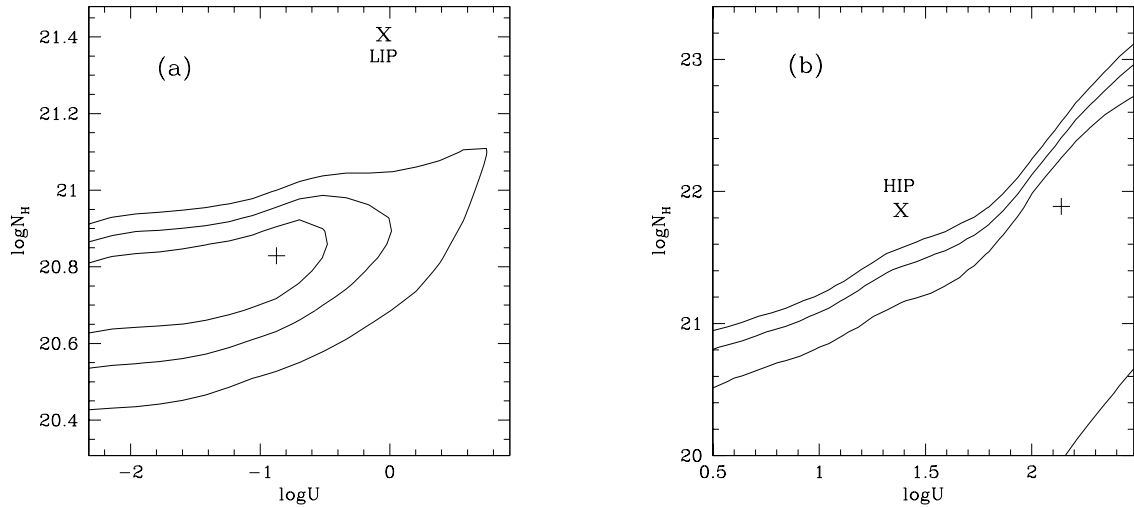


Fig. 10.— Confidence regions constraining the presence of a third absorber in the *Chandra* spectrum of NGC 985. The solid lines correspond to the  $1\sigma$ ,  $2\sigma$ , and  $3\sigma$  levels. Panel (a): A low ionization absorber with low column density ( $\log U = -1.0$  and  $\log N_{\text{H}} = 20.8$  [cm $^{-2}$ ]). Panel (b): A high ionization component with high column ( $\log U = 2.1$  and  $\log N_{\text{H}} = 21.8$  [cm $^{-2}$ ]).

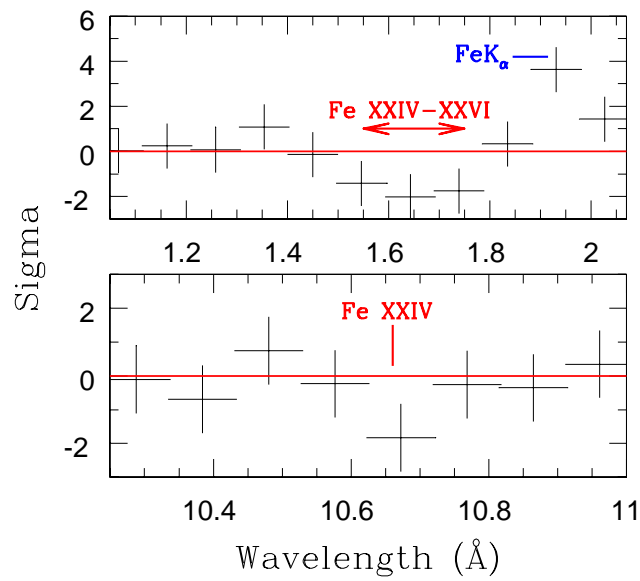


Fig. 11.— Residuals to our best fit model over *Chandra* data in the ranges 1.1-2 Å and 10.2-11 Å. The presence of absorption by material with significant amounts of Fe XXIV-XXVI is suggested in the figure, but better S/N ratio is required to constrain the physical properties of such component. [See the electronic edition of the Journal for a color version of this figure]

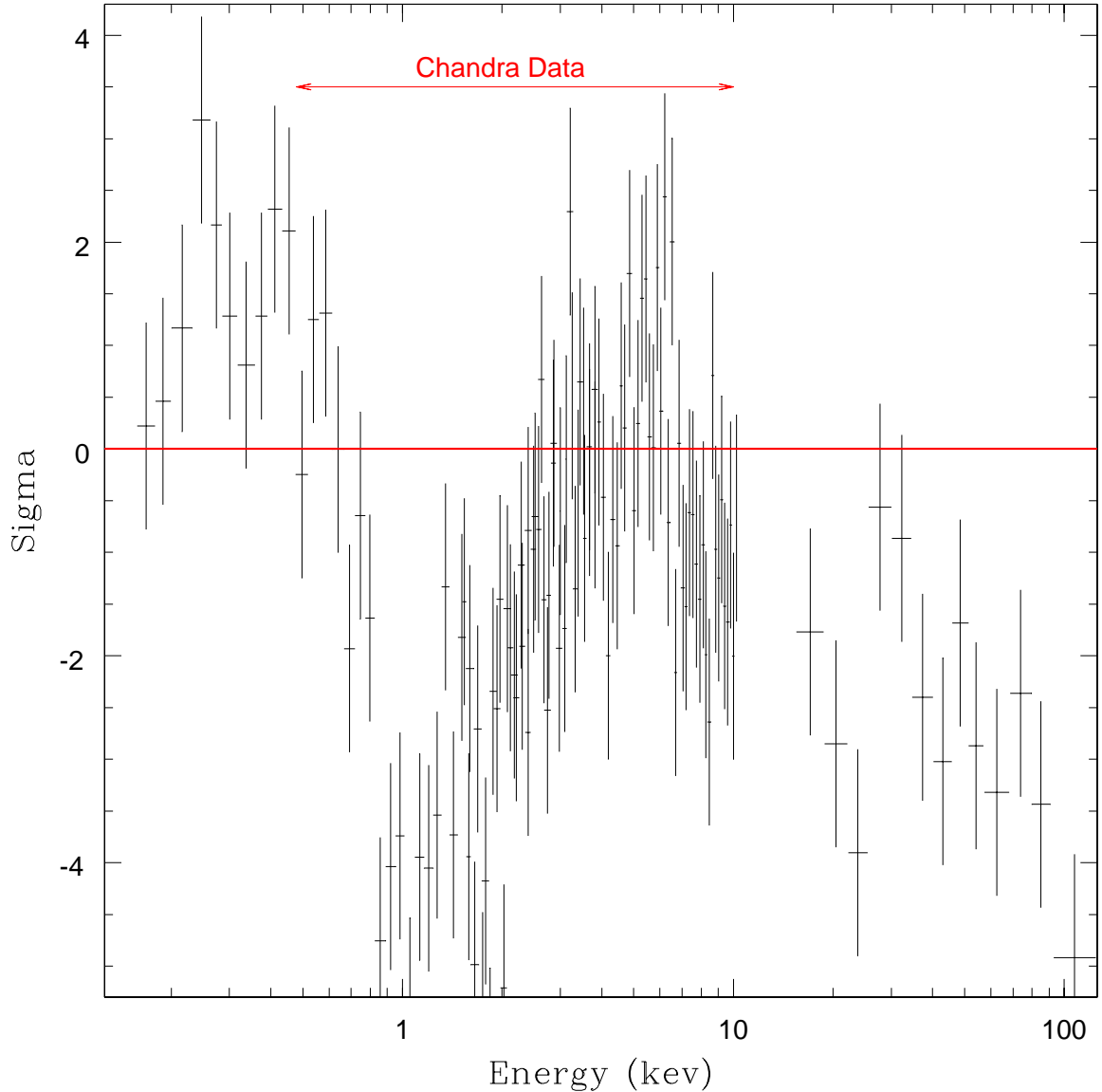


Fig. 12.— Fit residuals for a model including only a continuum power law constrained in the 3-8 keV range and further attenuated by Galactic absorption, over BeppoSAX data of NGC 985. [See the electronic edition of the Journal for a color version of this figure]

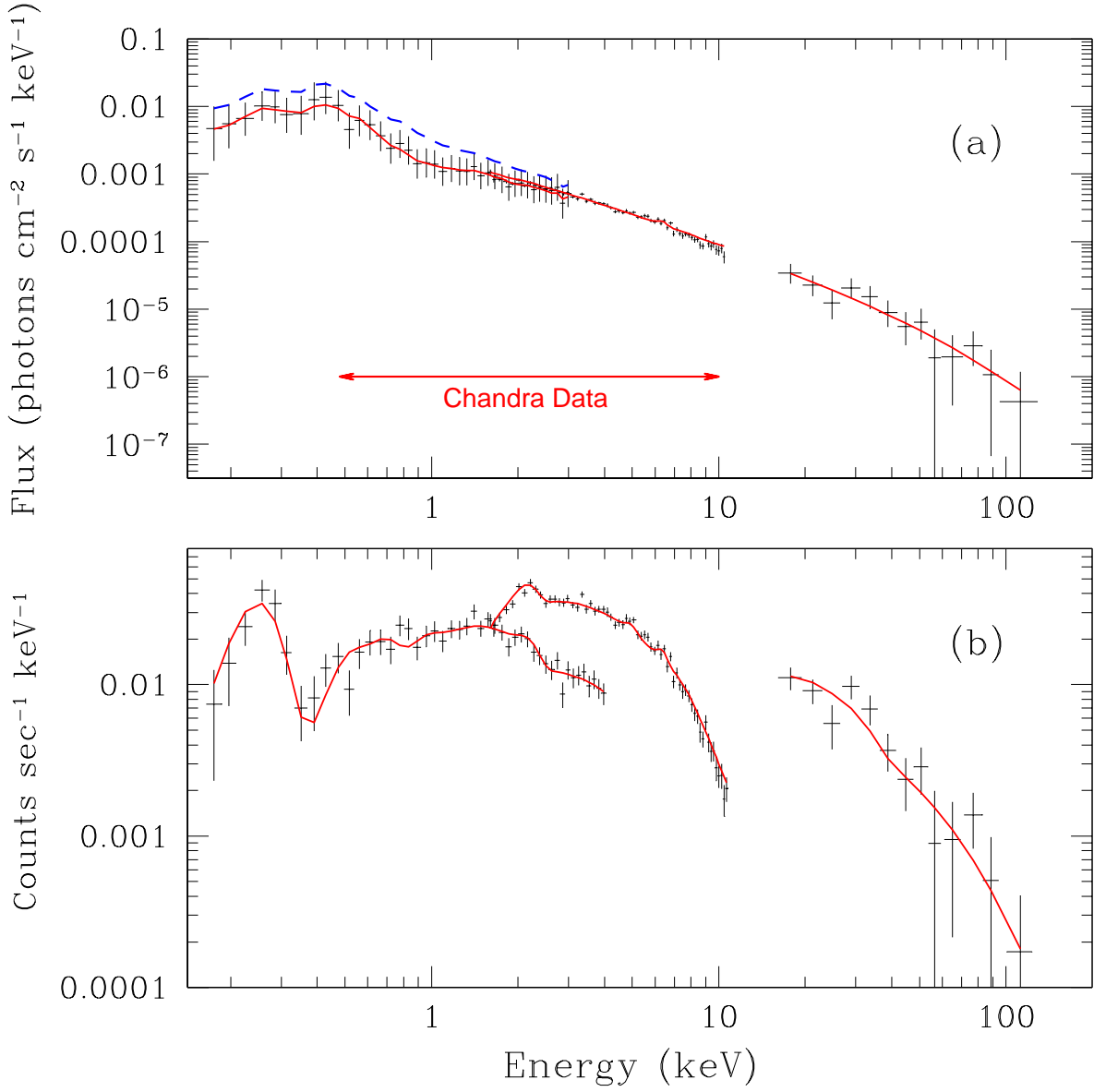


Fig. 13.— BeppoSAX spectra of NGC 985, plotted against an ionized absorber model for comparison. (a) Fluxed spectrum. The blue dashed line shows the continuum further attenuated by Galactic absorption. (b) Empirical Spectrum. [See the electronic edition of the Journal for a color version of this figure]

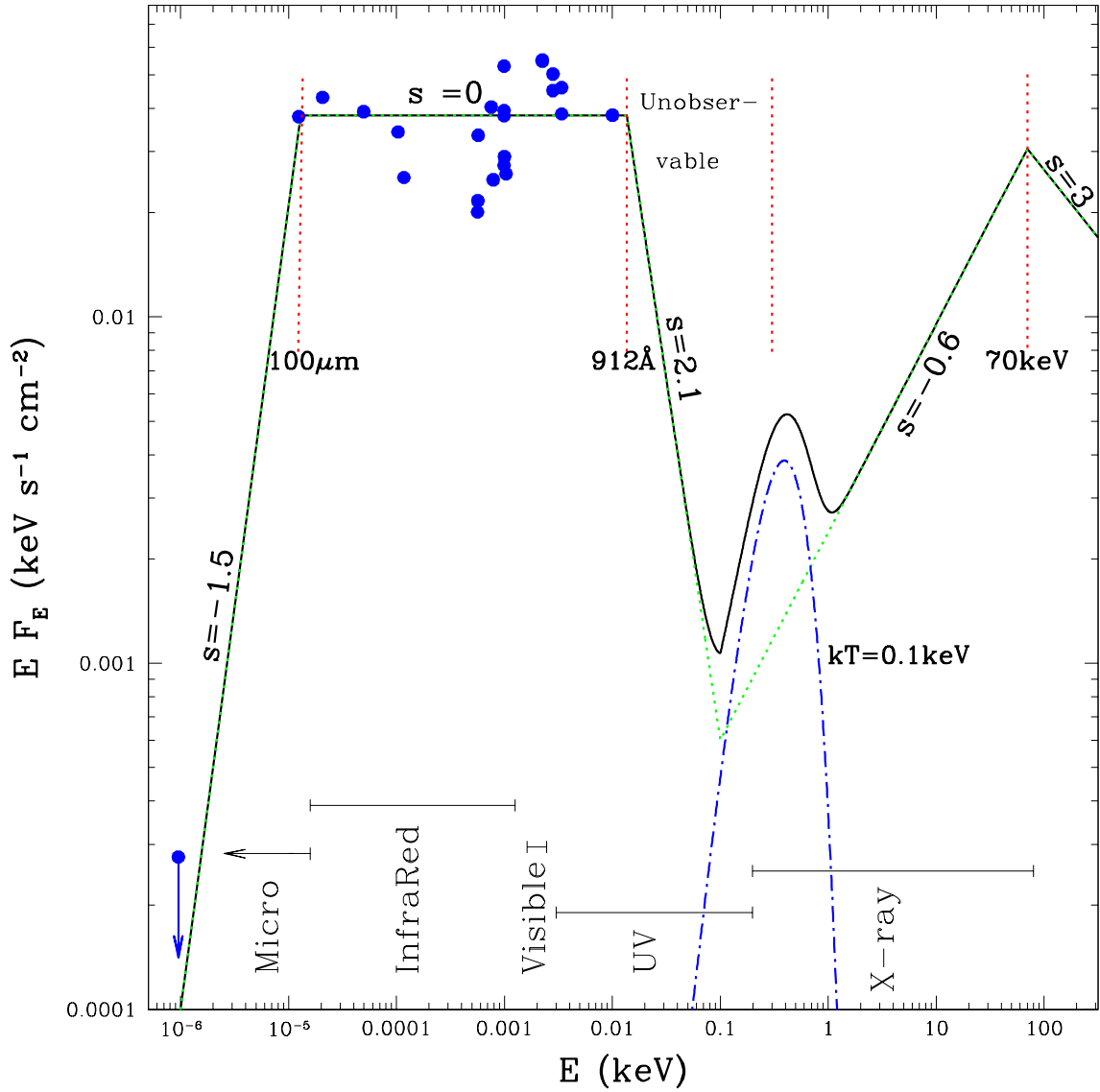


Fig. 14.— Spectral Energy Distribution used to model the ionized absorber observed in the BeppoSAX spectrum. Filled circles (blue) mark the observed SED of NGC 985 (obtained from NED). The plot shows the slope adopted in each energy range. This slope relates to the photon index as  $\Gamma = s + 2$ . The model assumes a low energy far UV cutoff at 0.1 keV and includes the contribution of a blackbody component. [See the electronic edition of the Journal for a color version of this figure]

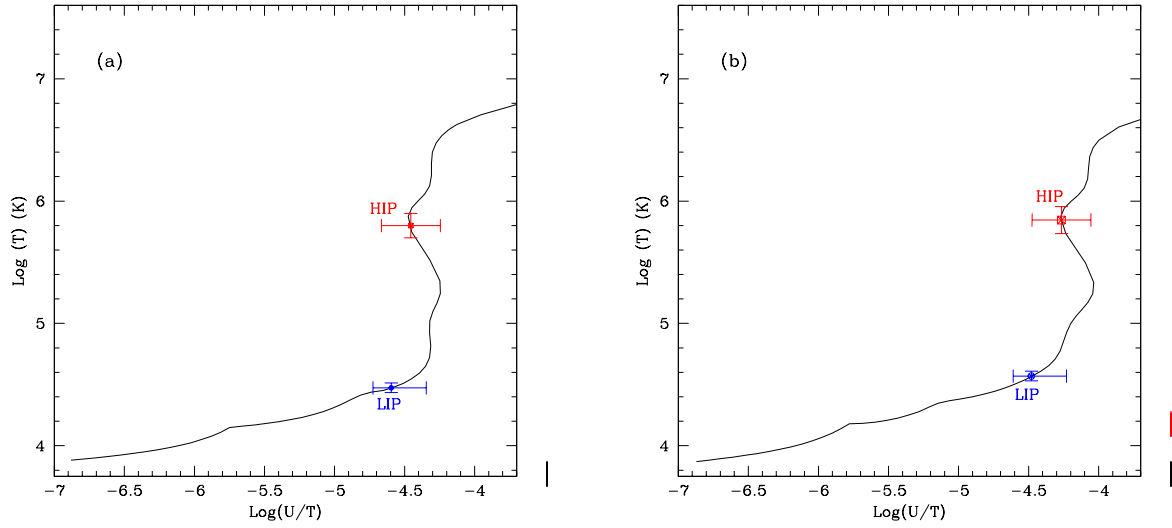


Fig. 15.— Curve of thermal stability for the two different SEDs used in the analysis of *Chandra* data, as described in the text. (a) Far UV cutoff at 0.1 keV plus blackbody (Fig. 3a). (b) Far UV cutoff at 1 keV (Fig. 3b). The positive error bar of the LIP represents the maximum effect in U induced by the lack of low temperature DRR. The HIP and the LIP are consistent with pressure equilibrium. [See the electronic edition of the Journal for a color version of this figure]

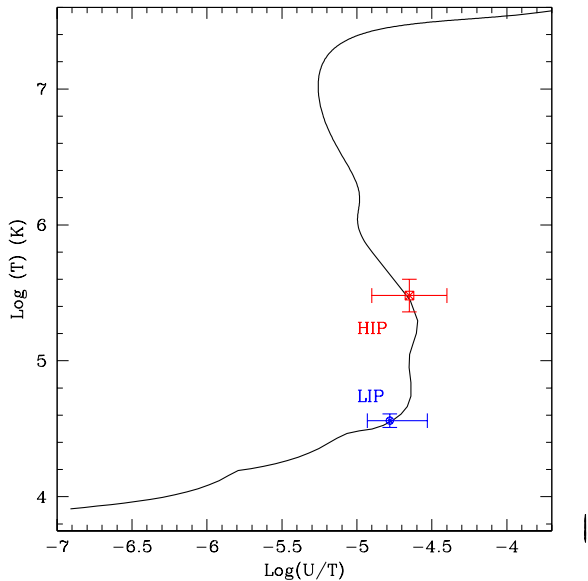


Fig. 16.— Curve of thermal stability for the SED used in the BeppoSAX analysis, as described in the text. The positive error bar of the LIP represents the maximum effect in  $U$  induced by the lack of low temperature DRR. Pressure balance between the LIP and the HIP appears to be present in the BeppoSAX data, even though the ionization degree of the gas is different than the one obtained for *Chandra* data, (see text for details). [See the electronic edition of the Journal for a color version of this figure]

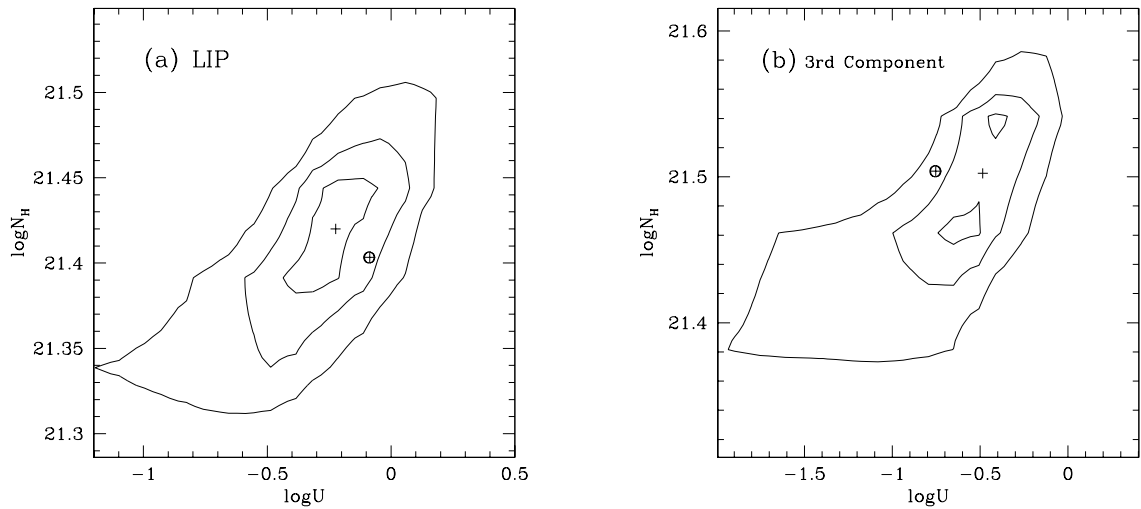


Fig. 17.— U vs.  $N_H$  confidence regions for a model fitted to simulated data including 3 absorption components: the HIP and LIP from the *Chandra* best fit model plus a third colder absorption component with  $\log U = -0.8$  and  $\log N_H = 21.5$  [ $\text{cm}^{-2}$ ]. The solid lines correspond to the  $1\sigma$ ,  $2\sigma$ , and  $3\sigma$  levels. In both panels the crossed-circle point marks the value used to produce the simulated data and the cross point marks the value obtained in the model. Panel (a): Confidence region for the LIP. Panel (b): Confidence region for the third component. Clearly, a third component would be detectable in the data, however, the ionization state of such a component would be difficult to constrain.

## REFERENCES

Appleton, P. N., Charmandaris, V., Gao, Y., Combes, F., Ghigo, F., Horellou, C., & Mirabel, I. F. 2002, ApJ, 566, 682

Arav, N. 2002, X-ray Spectroscopy of AGN with Chandra and XMM-Newton, 153

Arav, N., Kaastra, J., Steenbrugge, K., Brinkman, B., Edelson, R., Korista, K.T., Kool, & M. 2003, ApJ accepted(astro-ph/0303425)

Arribas, S., Mediavilla, E., del Burgo, C., & García-Lorenzo, B. 1999, ApJ, 511, 680

Behar, E., Rasmussen, A. P., Blustin, A. J., Sako, M., Kahn, S. M., Kaastra, J. S., Branduardi-Raymont, G., & Steenbrugge, K. C. 2003, ApJ, 598, 232

Behar, E., Sako, M., & Kahn, S. M. 2001, ApJ, 563, 497

Blustin, A. J., Branduardi-Raymont, G., Behar, E., Kaastra, J. S., Kahn, S. M., Page, M. J., Sako, M., & Steenbrugge, K. C. 2002, A&A, 392, 453

Blustin, A. J., et al. 2003, A&A, 403, 481

Boella, G., Butler, R. C., Perola, G. C., Piro, L., Scarsi, L., & Bleeker, J. A. M. 1997, A&AS, 122, 299

Bowen, D. V., Pettini, M., & Blades, J. C. 2002, ApJ, 580, 169

Brandt, W. N., Fabian, A. C., Nandra, K., Reynolds, C. S., & Brinkmann, W. 1994, MNRAS, 271, 958

Canizares, C.R., et al. 2000 ApJ, 539, L41

Crenshaw, D. M., Kraemer, S. B., Boggess, A., Maran, S. P., Mushotzky, R. F., & Wu, C. 1999, ApJ, 516, 750

Czerny, B. & Elvis, M. 1987, ApJ, 321, 305

de Rosa, A., Piro, L., Fiore, F., Grandi, P., Maraschi, L., Matt, G., Nicastro, F., & Petrucci, P. O. 2002, A&A, 387, 838

de Vaucouleurs, G. & de Vaucouleurs, A. 1975, ApJ, 197, L1

Elvis, M. 2000, ApJ, 545, 63

Elvis, M., Wilkes, B. J., Giommi, P., & McDowell, J. 1991, ApJ, 378, 537

Erkens, U., Appenzeller, I., & Wagner, S. 1997, A&A, 323, 707

Freeman, P., Doe, S., & Siemiginowska, A. 2001, Proc. SPIE, 4477, 76

Fruscione, A. 2002, *Chandra* News, 9, 20

Gabel, J. R. et al. 2003, ApJ, 583, 178

Garmire, G. P., Bautz, M. W., Ford, P. G., Nousek, J. A., & Ricker, G. R. 2003, Proc. SPIE, 4851, 28

George, I. M., Turner, T. J., Netzer, H., Nandra, K., Mushotzky, R. F., & Yaqoob, T. 1998, ApJS, 114, 73

George, I. M., Mushotzky, R., Turner, T. J., Yaqoob, T., Ptak, A., Nandra, K., & Netzer, H. 1998, ApJ, 509, 146

Grevesse, N., Noels, A., & Sauval, A. J. 1993, A&A, 271, 587

Gu, M. F. 2003, ApJ, 590, 1131

Halpern, J. P. 1984, ApJ, 281, 90

Kaastra, J. S., Steenbrugge, K. C., Raassen, A. J. J., van der Meer, R. L. J., Brinkman, A. C., Liedahl, D. A., Behar, E., & de Rosa, A. 2002, *A&A*, 386, 427

Karovska, M., Fabbiano, G., Nicastro, F., Elvis, M., Kraft, R. P., & Murray, S. S. 2002, *ApJ*, 577, 114

Kaspi, S. et al. 2002, *ApJ*, 574, 643

Kaspi, S. et al. 2001, *ApJ*, 554, 216

Kinkhabwala, A., et al. 2002, *ApJ*, 575, 732

Komossa, S. & Fink, H. 1997, *A&A*, 322, 719

Kraemer, S. B., Ferland, G. J., & Gabel, J. R. 2003, ArXiv Astrophysics e-prints, astro-ph/0311568

Kriss, G. A., Blustin, A., Branduardi-Raymont, G., Green, R. F., Hutchings, J., & Kaiser, M. E. 2003, *A&A*, 403, 473

Krolik, J. H. & Kriss, G. A. 2001, *ApJ*, 561, 684

Krolik, J. H., McKee, C. F., & Tarter, C. B. 1981, *ApJ*, 249, 422

Krongold, Y., Nicastro, F., Brickhouse, N.S., Elvis, M., Liedahl D.A. & Mathur, S. 2003, *ApJ*, 597, 1

Kruper, J. S., Canizares, C. R., & Urry, C. M. 1990, *ApJS*, 74, 347

Marshall, H. L., Tennant, A., Grant, C. E., Hitchcock, A. P., O'Dell, S., & Plucinsky, P. P. 2003, ArXiv Astrophysics e-prints, astro-ph/0308332

Mathur, S., Elvis, M., & Wilkes, B. 1995, *ApJ*, 452, 230

Mathur, S., Wilkes, B., & Elvis, M. 1998, *ApJ*, 503, L23

Monier, E. M., Mathur, S., Wilkes, B., & Elvis, M. 2001, *ApJ*, 559, 675

Netzer, H. 1996, *ApJ*, 473, 781

Netzer, H., Chelouche, D., George, I. M., Turner, T. J., Crenshaw, D. M., Kraemer, S. B., & Nandra, K. 2002, *ApJ*, 571, 256

Netzer, H., et al. 2003, *ApJ*, 599, 933

Netzer, H. 2004, *ApJ*, 604, 551

Nicastro, F., Fiore, F., Brandt, N., & Reynolds, C. S. 1998, The Active X-ray Sky: Results from BeppoSAX and RXTE, 501

Nicastro, F., Fiore, F., Perola, G. C., & Elvis, M. 1999, *ApJ*, 512, 184

Nicastro, F., Fiore, F., & Matt, G. 1999, *ApJ*, 517, 108

Ogle, P. M., Mason, K. O., Page, M. J., Salvi, N. J., Cordova, F. A., McHardy, I. M., & Priedhorsky, W. C. 2004, ArXiv Astrophysics e-prints, astro-ph/0401173

Perez Garcia, A. M.. & Rodriguez Espinosa, J. M. 1996, *AJ*, 112, 1863

Piro, L. & The BeppoSAX Collaboration 1997, AIP Conf. Proc. 410: Proceedings of the Fourth Compton Symposium, 410, 1485

Reynolds, C. S. 1997, *MNRAS*, 286, 513

Sako, M. et al. 2001, A&A, 365, L168

Savin, D. W., et al. 2003, ApJS, 147, 421

Savin, D. W., et al. 2002a, ApJ, 576, 1098

Savin, D. W., et al. 2002b, ApJS, 138, 337

Shull, J. M. & van Steenberg, M. 1982, ApJS, 48, 95

Starck, J., Siebenmorgen, R., & Gredel, R. 1997, ApJ, 482, 1011

Steenbrugge, K. C., et al. 2003, A&A, 408, 921

Steenbrugge, K. C., Kaastra, J. S., de Vries, C. P., & Edelson, R. 2003, A&A, 402, 477

Weisskopf, M. C., Tananbaum, H. D., Van Speybroeck, L. P., & O'Dell, S. L. 2000, Proc. SPIE, 4012, 2